PHILOSOPHICAL TRANSACTIONS OF THE ROYAL SOCIETY A MATHEMATICAL, PHYSICAL & ENGINEERING SCIENCES

Bloch Wave Degeneracies in Systematic High Energy Electron Diffraction

B. F. Buxton and M. V. Berry

Phil. Trans. R. Soc. Lond. A 1976 **282**, 485-525
doi: 10.1098/rsta.1976.0062

BLOCH WAVE DEGENERACIES IN SYSTEMATIC HIGH ENERGY ELECTRON DIFFRACTION

By B. F. Buxton and M. V. Berry
H. H. Wills Physics Laboratory, Tyndall Avenue, Bristol BS8 1TL

(*Communicated by J. M. Ziman, F.R.S. – Received 15 October 1975*)

CONTENTS

Vol. 282. A 1308. 31 [Published 13 July 1976

For the systematic diffraction of high energy electrons by a thin crystalline slab, we study the accidental degeneracies of the Bloch waves excited in the specimen by the incident beam. It is shown that these Bloch waves are the eigenstates of a one dimensional band structure problem, and this is solved by wave matching methods. For a symmetric potential, the symmetry properties of the Bloch waves are discussed, and it is shown how accidental degeneracies of these waves can occur when the reflexion coefficient for waves incident on one unit cell of the one dimensional periodic potential vanishes. The form of the band structure and the Bloch waves in the neighbourhood of a degeneracy are derived by expanding the Kramers function in a Taylor series. It is then shown analytically how the degeneracy affects the diffracted waves emerging from the crystalline specimen (in particular, the Kikuchi pattern). To understand these effects fully, W.K.B. approximations for the Bloch waves are used to derive the Bloch wave excitations and the absorption coefficients. However, to predict the degeneracies themselves, it is shown that a different formula for the reflexion coefficient, due to Landauer, must be used. This formula shows how the critical voltage at which the Bloch waves degenerate depends on the form of the potential, and allows quick, accurate, computations of the critical voltages to be made. Also, a new higher order degeneracy is predicted for some of the systematic potentials of cadmium, lead and gold. Finally, to infer the potential in real space from measurements of critical voltages and several other quantities, we suggest an inversion scheme based on the Landauer formula for the reflexion coefficient. To a close approximation this potential is proportional to ∇^2 of the crystal charge density.

1. Introduction

A few years ago, Nagata & Fukuhara (1967) found that, in the (222) dark field image of a bent wedge-shaped aluminium specimen, the intensity of the second order (222) line became a minimum at a certain 'critical' incident electron accelerating voltage. They immediately recognized that this effect was due to the accidental degeneracy of two of the Bloch waves excited in the crystal and predicted that the phenomenon should occur quite often under systematic diffraction conditions. A little later (Watanabe, Uyeda & Fukuhara 1968; Watanabe, Uyeda & Kogiso 1968), it was discovered that at the same 'critical voltage', the second order Kikuchi line vanished and that the central, displaced Kikuchi line reversed its sense of asymmetry. Although these critical voltage effects have frequently been used since then to measure atomic scattering factors and other properties of the crystalline specimen (see, for example, Lally, Humphreys, Metherell & Fisher 1972; Thomas, Shirley, Lally & Fisher 1973), a study of all the possible degeneracies which may occur at the Bragg positions under systematic diffraction conditions has not previously been published.

We study these degeneracies by relating the diffraction problem to a one dimensional band structure (Berry 1971) and solve the latter in real space by wave matching methods. We also introduce a number of analytic semiclassical approximations which enable us to predict which Bloch waves can degenerate and how the degeneracy affects the diffracted waves emerging from the crystalline specimen. Moreover, the simplicity and accuracy of these approximations enable us to devise an inversion technique for inferring the potential in real space directly from critical voltage and critical angle measurements (Berry, Buxton & Ozorio de Almeida 1973; Buxton & Berry 1973). By combining these reconstructed one dimensional potentials, a three dimensional potential is obtained. Dederichs (1972) showed that this is closely proportional to ∇^2 of the thermally averaged crystal charge density.

In § 2 we introduce the one dimensional band structure problem and discuss the symmetry properties of the Bloch eigenstates for a symmetric potential. Degeneracies of these Bloch waves

at the Bragg positions are associated with resonances in the transmission of waves through the potential barrier formed from a single unit cell of the periodic potential, and it is shown how the parities of the non-degenerate Bloch waves depend on the form of the transmission and reflexion coefficients. In § 3 we derive the form of the band structure, of the Bloch waves and of their Fourier coefficients, in the neighbourhood of a degeneracy and show how this affects the diffracted waves and the Kikuchi pattern. The semiclassical approximations are used in § 4 to discuss these effects further and to predict qualitatively which Bloch waves can degenerate for a given potential, and at what voltage. In § 5, we show that the same formulae can be used to compute critical voltages very accurately, and to follow the behaviour of critical voltages as the temperature of the specimen is varied. A new type of 'higher-order' degeneracy, at which the parities of the degenerate waves are not interchanged, is discovered and explained. This quantitative success of the semiclassical approximations means that we can devise an approximate inversion technique to obtain the potential from critical voltage and critical angle measurements, and this is presented in § 6. We show also that when combined with information relating to extinction distances this technique can be made quite precise.

2. The one dimensional eigenvalue problem

Neglecting spin effects (Fujiwara 1961, 1962), we use the relativistic Schrödinger equation

$$\left[\nabla^2 + k_0^2 - \frac{2mV(\boldsymbol{r})}{\hbar^2}\right]\psi(\boldsymbol{r}) = 0 \tag{2.1}$$

to describe the elastic scattering by a crystal of fast electrons with rest mass m_0. $V(\boldsymbol{r})$ is the periodic potential energy function of an electron in the crystal and k_0 is the wavenumber $2\pi/\lambda$, given by

$$k_0 = (m_0 c/\hbar)\sqrt{(\gamma^2 - 1)}, \quad \gamma = m/m_0 = 1 + E/m_0 c^2, \tag{2.2}$$

where γ is the relativistic increase in mass of the electrons which have been accelerated through a potential of E (kV). We suppose that the incident electron beam (regarded as a plane wave $e^{ik_0 \cdot r}$) is nearly parallel to the z axis and impinges on a thin slab of crystal, so oriented that only one row of reciprocal lattice points lies near the Ewald sphere. It has been shown (Berry 1971) that under these circumstances, if z is normal to the surfaces of our slab of crystal, we may replace $V(\boldsymbol{r})$ by $\bar{V}(x)$, which is its average over a plane normal to a reciprocal lattice row; this row is taken as the x axis and is assumed to lie in a plane parallel to the surfaces of the slab. In this case of *systematic diffraction*, $\bar{V}(x)$, which has a period a (say), is given by the Fourier series:

$$\bar{V}(x) = \sum_G V_G e^{iGx}, \tag{2.3}$$

where $G = 2\pi n/a$, and n is an integer.

We solve (2.1) by expanding $\psi(\boldsymbol{r})$ as a sum of Bloch waves which have constant total energy but slightly differing kinetic energies. Writing $\bar{U}(x)$ for $2m\bar{V}(x)/\hbar^2$, replacing $V(\boldsymbol{r})$ by $\bar{V}(x)$ and substituting the expansion

$$\psi(\boldsymbol{r}) = \frac{1}{\sqrt{a}} \sum_j b_0^{(j)*} \tau_j(x)\, e^{ik_z^{(j)} z}, \tag{2.4}$$

in (2.1), we find that the $\tau_j(x)$ are eigenfunctions of a one dimensional Schrödinger equation:

$$[-d^2/dx^2 + \bar{U}(x)]\,\tau_j(x) = s_j \tau_j(x), \tag{2.5}$$

where

$$k_0^2 - k_z^{(j)2} \equiv s_j. \tag{2.6}$$

Since the $k_z^{(j)2}$ differ only slightly from k_0^2 and backwards travelling waves may be neglected for the energy range of interest ($E \gtrsim 40\,\mathrm{kV}$), we can write

$$k_z^{(j)} \approx k_0 - s_j/2k_0. \tag{2.7}$$

The details have been given by Berry (1971), who shows that matching the waves inside the crystal to the incident plane wave $\mathrm{e}^{\mathrm{i}\boldsymbol{k}_0\cdot\boldsymbol{r}}$ at the top surface of the slab at $z = 0$ determines the wavenumber K_0 of the one dimensional Bloch waves $\tau_j(x)$, and their excitation amplitudes $b_0^{(j)*}$. K_0 is just the component of $\boldsymbol{k}_0$ along the x axis and is therefore a measure of the tilt of the incident beam along the systematic row. Moreover, if the $\tau_{jK_0}(x)$ (where we now write the K_0 dependence explicitly) are normalized over a unit cell a, the excitation amplitude of the jth Bloch wave is, as anticipated above, the complex conjugate of the zero order Fourier coefficient of the Bloch wave. The general coefficients $b_G^{(j)}$ are defined by

$$b_G^{(j)}(K_0) \equiv \frac{1}{\sqrt{a}} \int_{-\frac{1}{2}a}^{\frac{1}{2}a} \mathrm{d}x\, \tau_{jK_0}(x)\, \mathrm{e}^{-\mathrm{i}(K_0+G)x}. \tag{2.8}$$

Berry (1971) has also written the wavefunction $\psi(\boldsymbol{r})$ as a sum over diffracted waves

$$A_G(K_0, z)\, \mathrm{e}^{\mathrm{i}(K_0+G)x}\, \mathrm{e}^{\mathrm{i}k_0 z}$$

and shown that

$$A_G(K_0, z) = \sum_j b_0^{(j)*} b_G^{(j)}\, \mathrm{e}^{-\mathrm{i}s_j z/2k_0}. \tag{2.9}$$

(a) *The one dimensional Bloch waves*

Usually, in the 'many-beam' formulation of high energy electron diffraction (see, for example, Hirsch *et al.* 1965), the one dimensional band structure problem (2.5) is solved by expanding the potential and the Bloch waves $\tau_{jK_0}(x)$ in Fourier series, a process which leads to the usual algebraic eigenvalue problem

$$[s_j - (K_0+G)^2]\, b_G^{(j)} - \sum_{G'} U_{G-G'}\, b_{G'}^{(j)} = 0, \tag{2.10}$$

where U_G is $2mV_G/\hbar^2$. However, it is also well known (Kramers 1935; Kohn 1959; Jones 1960; Scharff 1969) that (2.5) can be solved by wave matching methods. For a symmetric potential, $\bar{U}(x) = \bar{U}(-x)$ (we choose the origin of x to be at one of the highest maxima of $\bar{U}(x)$ and take $\bar{U}(0)$ as zero), we may express $\tau_{jK_0}(x)$ in terms of real even and odd functions $\tau_\mathrm{e}(x)$ and $\tau_\mathrm{o}(x)$ respectively, which are themselves solutions of (2.5) for a given s. Writing

$$\tau_{jK_0}(x) = A_j(K_0)\, \tau_\mathrm{e}(x) + \mathrm{i}B_j(K_0)\, \tau_\mathrm{o}(x), \tag{2.11}$$

the energy bands $s_j(K_0)$ are determined from

$$\cos(K_0 a) = \mu(s, \gamma) \equiv \left.\frac{\tau_\mathrm{e}\tau_\mathrm{o}' + \tau_\mathrm{o}\tau_\mathrm{e}'}{\tau_\mathrm{e}\tau_\mathrm{o}' - \tau_\mathrm{o}\tau_\mathrm{e}'}\right|_{x=\frac{1}{2}a}, \tag{2.12}$$

and the coefficients $A_j(K_0)$, $B_j(K_0)$ from

$$\frac{A_j}{B_j} = \frac{\tau_\mathrm{o}(\frac{1}{2}a)}{\tau_\mathrm{e}(\frac{1}{2}a)} \cot(\tfrac{1}{2}K_0 a) = -\frac{\tau_\mathrm{o}'(\frac{1}{2}a)}{\tau_\mathrm{e}'(\frac{1}{2}a)} \tan(\tfrac{1}{2}K_0 a). \tag{2.13}$$

We have stressed the dependence of μ on the relativistic factor γ, because as the incident beam accelerating voltage is changed, the potential $\bar{U}(x) = \gamma\bar{U}_0(x)$ (say) becomes deeper and the nature of the solutions changes.

Alternatively, these even and odd functions can be expressed in terms of travelling waves $\tau_\mathrm{L}(x)$ and $\tau_\mathrm{R}(x)$ incident from the left and right on one cell of the potential as shown in figure 1.

For a symmetric potential barrier we may write the transmission and reflexion coefficients in the form

$$T = |T|\,e^{i\delta}, \quad R = i\,|R|\,e^{i(\delta+p\pi)}, \tag{2.14}$$

in the region where $\sqrt{[s-\bar{U}(\frac{1}{2}a)]}$, the wavenumber β at the edge of the unit cell, is real (see, for example, Messiah 1962, vol. 1). The significance of the integer p will be discussed in § 2 (*b*). It is then fairly easy to show (Berry 1971) that

$$\mu(s,\gamma) = \frac{\cos(\beta a+\delta)}{|T|} \equiv \frac{\cos[\Phi(s,\gamma)]}{|T|}. \tag{2.15}$$

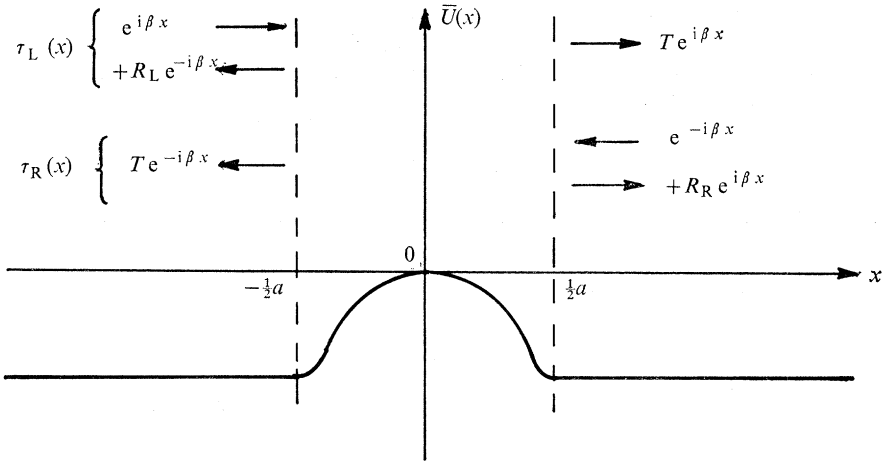

FIGURE 1. Waves incident from the left and right and transmitted and reflected by the potential in a unit cell. For a symmetric potential barrier there is no distinction between left and right and there is only one reflexion coefficient, R.

It is obvious from (2.12) that $s_j(K_0)$ is periodic with period $2\pi/a$, and it follows from (2.8), (2.11) and (2.13) that for any wavenumber H which is an integral multiple of $2\pi/a$ we can write

$$\frac{\tau_{jK_0+H}(x)}{\tau_{jK_0}(x)} \equiv \alpha_p^{(j)}(H) = \frac{A_j(K_0+H)}{A_j(K_0)} = \frac{B_j(K_0+H)}{B_j(K_0)} = \frac{b_{G-H}^{(j)}(K_0+H)}{b_G^{(j)}(K_0)}; \tag{2.16}$$

if we make the convenient choice of A_j and B_j real for a symmetric potential, the phase factor $\alpha_p^{(j)}(H)$ is just (± 1). This is the periodicity relation (Metherell & Fisher 1969). Similarly, $s_j(K_0)$ is the same as $s_j(-K_0)$, and

$$\frac{\tau_{j-K_0}(x)}{\tau^*_{jK_0}(x)} \equiv \alpha_T^{(j)} = \frac{A_j(-K_0)}{A_j(K_0)} = -\frac{B_j(-K_0)}{B_j(K_0)} = \frac{b_{-G}^{(j)}(-K_0)}{b_G^{(j)}(K_0)}, \tag{2.17}$$

where $\alpha_T^{(j)}$ is again (± 1); this relation expresses time reversal invariance. Finally, it is well known that at the Bragg positions where $K_0 = K_0^B = m\pi/a$ (Jones 1960),

$$B\tau_o(\tfrac{1}{2}a) = 0 \quad \text{and} \quad A\tau'_e(\tfrac{1}{2}a) = 0 \tag{2.18}$$

if m is even (even Bragg position), whereas if m is odd (odd Bragg position),

$$A\tau_e(\tfrac{1}{2}a) = 0 \quad \text{and} \quad B\tau'_o(\tfrac{1}{2}a) = 0. \tag{2.19}$$

Thus at the Bragg positions the Bloch waves have a definite symmetry, unless by chance two are degenerate. Even if one of these accidental degeneracies occurs, we can still *choose* the relevant $\tau_{jK_0}(x)$ to be one even and one odd Bloch wave, so that at $K_0^{\mathrm{B}} = m\pi/a$ it is easily shown that

$$\frac{\tau_{j\frac{1}{2}mG_0}(x)}{\tau_{j\frac{1}{2}mG_0}(-x)} \equiv \epsilon_s^{(j)}(\tfrac{1}{2}mG_0) = \frac{b^{(j)}_{nG_0}(\frac{1}{2}mG_0)}{b^{(j)}_{(-n-m)G_0}(\frac{1}{2}mG_0)}, \tag{2.20}$$

where $G_0 \equiv 2\pi/a$ and $\epsilon_s^{(j)}(\frac{1}{2}mG_0)$ is $+1$ if $\tau_{j\frac{1}{2}mG_0}(x)$ is an even function and -1 if it is odd. It should be noted, however, that a shift of the origin of the unit cell by $\frac{1}{2}a$ changes $\epsilon_s^{(j)}(\frac{1}{2}mG_0)$ to $\epsilon_s^{(j)}(\frac{1}{2}mG_0)\,\mathrm{e}^{\mathrm{i}m\pi}$, so that the symmetries of the Bloch waves at the odd Bragg position are all changed. Also, fixing K_0 as $\frac{1}{2}mG_0$ and H as $-mG_0$, (2.16) and (2.17) may be compared and (2.20) used to derive the following relation between our symmetry properties:

$$\alpha_p^{(j)}(-mG_0) = \alpha_T^{(j)}\epsilon_s^{(j)}(\tfrac{1}{2}mG_0) \tag{2.21}$$

(this holds because either $A_j(\frac{1}{2}mG_0)$ or $B_j(\frac{1}{2}mG_0)$ is always zero). Finally, the choice of

$$\alpha_T^{(j)} = \epsilon_s^{(j)}(0) \tag{2.22}$$

guarantees that all of the A_j, B_j and $b_G^{(j)}$ are continuous and smooth functions of K_0.

(*b*) *The symmetries of the one dimensional Bloch waves at the Bragg positions*

By considering the transmission and reflexion coefficients introduced earlier we can determine quite simply the order of the symmetries of the Bloch waves for increasing s_j, provided s exceeds $\bar{U}(\frac{1}{2}a)$. If the functions are suitably normalized, we can arrange matters so that

$$\left.\begin{aligned}\tau_{\mathrm{e}} &= \tfrac{1}{2}(\tau_{\mathrm{L}}+\tau_{\mathrm{R}}),\\ \tau_{\mathrm{o}} &= \frac{1}{2\mathrm{i}}(\tau_{\mathrm{L}}-\tau_{\mathrm{R}}).\end{aligned}\right\} \tag{2.23}$$

For instance, at an even Bragg position, if the Bloch wave is to have even parity we see from (2.18) that $\tau_{\mathrm{e}}'(\frac{1}{2}a)$ is zero, from which we can show, using (2.14) and (2.23) that

$$|R| = -(\sin\Phi/\cos\pi p), \tag{2.24}$$

while if the Bloch wave is to be of odd parity

$$|R| = +(\sin\Phi/\cos\pi p). \tag{2.25}$$

At an odd Bragg position the situation is similar; we obtain equations (2.24) and (2.25) again, except that the former applies to an odd Bloch wave and the latter to an even Bloch wave.

Now what is the integer p? For $s > \bar{U}(\frac{1}{2}a)$, $T(s)$ is never zero or infinite for the finite potential barriers of interest here and we may assume that both $|T(s)|$ and $\delta(s)$ are smoothly varying functions of s. For $s > 0$, $|T(s)|$ can be unity as shown in figure 2 at transmission resonances (see, for example, Messiah (1962), vol. 1), so that $|R(s)|$ *can be zero*. If such a zero of R is of order r, a Taylor expansion of $R(s)$ about the zero shows that arg (R) changes abruptly by $r\pi$ as we pass through the zero. Elsewhere the phase of R will be smoothly varying in accordance with the $\delta(s)$ part of (2.14). For s only a little greater than $\bar{U}(\frac{1}{2}a)$ let us assume that the value of p is q'; then as we increase s the phase of R varies smoothly with s until we pass a transmission resonance where the phase suddenly increases by $r\pi$ and p becomes $q'+r$. Thus, if q is the number of zeros of $R(s')$ for $\bar{U}(\frac{1}{2}a) < s' < s$, $p(s)$ is $q'+q$. Since the eigenvalues s_j are the solutions of

$$|T(s)| = \pm\cos(\Phi(s)) \tag{2.26}$$

at even (+) and odd (−) Bragg positions, a knowledge of the symmetry of one state with $s_j > \bar{U}(\frac{1}{2}a)$, together with the positions of the zeros of $R(s)$, will determine the symmetries of all the states with $s_j > \bar{U}(\frac{1}{2}a)$ as shown in figure 2.

The important point is that the symmetry of a state with $s_j > 0$ depends on the relative positions of the peaks of $\cos(\Phi(s))$ and $|T(s)|$ (Steeds & Enfield 1971). If a transmission resonance and a peak of $\cos(\Phi(s))$ coincide, our arguments above tell us nothing about the symmetries of the two degenerate states ($p(s)$ cannot be assigned), but as the peak of $\cos(\Phi(s))$ moves through a resonance the symmetries of the states n and $n+1$ will interchange as shown in figure 3. As we shall see in the next section, simply by varying the accelerating voltage of the incident electrons we can alter the relative positions of these curves, because of the dependence of $\bar{U}(x)$ on the relativistic factor γ.

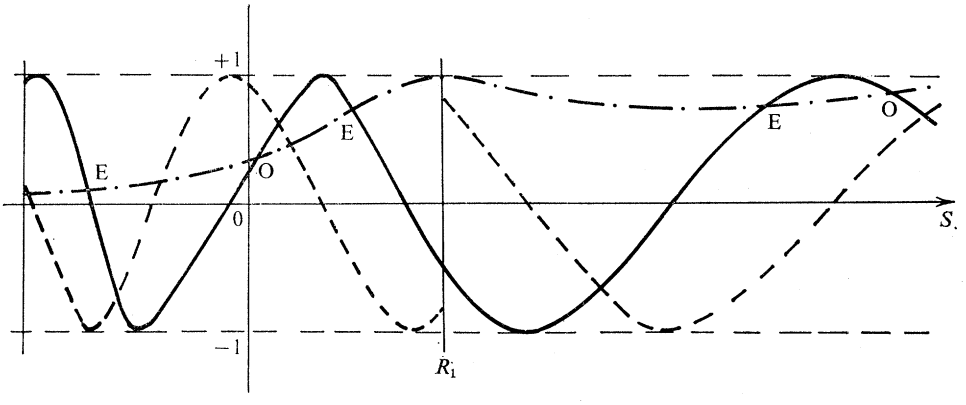

FIGURE 2. A sketch of $\cos(\Phi(s))$ (——), $|T(s)|$ (—·—) and $\sin(\Phi(s))/\cos(\pi p)$ (------) as functions of s. The letters E and O indicate the position of the eigenvalues at an even Bragg orientation and the symmetry of the corresponding Bloch wave, E for even, O for odd. The lowest state has been taken as of even parity, so q' is unity and $p = 1$ below the first resonance R_1, above which $p = 2$, etc.

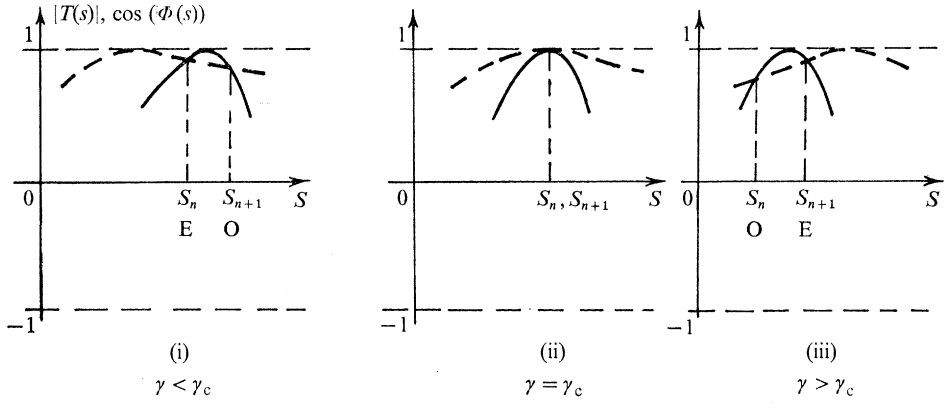

FIGURE 3. The sketches show the peak in $\cos(\Phi(s))$ (——), passing through a transmission resonance of $|T(s)|$ (------), so that the symmetries of states n and $n+1$ (say) are interchanged. The argument summarized in this figure was suggested to us by Dr J. W. Steeds.

If it is possible to represent the symmetric 'scattering potential' as a single barrier, so that the lowest value of the potential is $\bar{U}(\frac{1}{2}a)$ as in figure 1, it is easy to go a little further. At an even Bragg position where the Bloch waves have the same sign in corresponding regions in each cell, inspection of the differential equation (2.5) leads us to expect that there will be an eigenstate τ_1 which has no nodes. All other eigenstates τ must have nodes, so they are orthogonal to τ_1 and it is then

easy to apply the Wronksian theorem (see, for example, Messiah (1962), vol. 1) between consecutive zeros of τ and show that s_1 is less than the eigenenergy s of τ. Moreover, since τ_1 has no zeros it must be an even function and $p(s_1)$ must be unity. At an odd Bragg position, the wave function changes sign from cell to cell and all Bloch waves must have nodes. There is therefore no quick way of determining the symmetry of the lowest state at an odd Bragg position: we must have a knowledge of the first solution of (2.26) and the first zero of $R(s)$. Comparison of equations (2.24), (2.25) and (2.26) shows that in this simple but important case the symmetry of the jth Bloch wave at the mth Bragg position is given by

$$\epsilon_s^{(j)}(m\pi/a) = (-1)^{j+m+q+1}, \tag{2.27}$$

where q is the number of zeros of $R(s')$ for $s' < s_j$, and the lowest state is labelled 1.

3. Bloch wave degeneracies

In the previous sections, we showed how the eigenvalues s_j (and hence the dispersion surface $k_z^{(j)}$) and the Bloch waves $\tau_{jK_0}(x)$ could be determined. We shall now use the function $\mu(s, \gamma)$ which was defined in (2.12), to investigate the neighbourhood of an accidental degeneracy of the Bloch waves. The form of $\mu(s, \gamma)$ as a function of s was determined by Kramers (1935) to be as shown in figure 4. In particular, he showed that, at the turning points μ_i, where $\partial\mu/\partial s\ (\equiv \mu_s)$ vanishes, $\mu_i^2 - 1$ is positive semi-definite. Using the same methods we choose the normalization of the even and odd basis functions $\tau_e(x)$ and $\tau_o(x)$ so that $\tau_e(0) = \tau_o'(0) = 1$. The Wronskian of these functions is then unity for all x, s and γ.

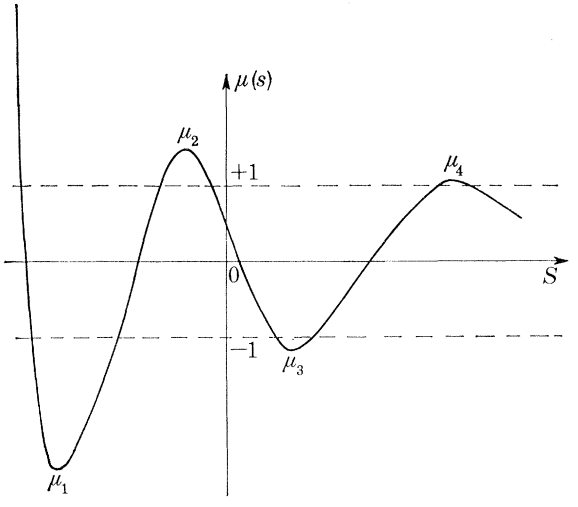

Figure 4. A sketch of the form of $\mu(s, \gamma)$ as a function of s. The turning point μ_i separates the bands labelled by s_i and s_{i+1}, since the lowest band is labelled as s_1 and the rest labelled in order of increasing s_j.

Differentiating the Schrödinger equation (2.5), and also the boundary conditions on τ_e and τ_o at $x = 0$, with respect to s, it is simple to use the method of variation of constants to evaluate the partial derivatives $\partial\tau_e(x)/\partial s$ and $\partial\tau_o(x)/\partial s$. We then find that

$$\partial\mu/\partial s \equiv \mu_s = 2[\tau_e\tau_e' I_{oo} - \tau_o\tau_o' I_{ee}], \tag{3.1}$$

where all the functions are to be evaluated at $\frac{1}{2}a$; the integrals I_{ee}, I_{oo} are given by:

$$\left.\begin{aligned} I_{ee} &\equiv \int_0^{\frac{1}{2}a} \mathrm{d}x\, \tau_e^2(x), \\ I_{oo} &\equiv \int_0^{\frac{1}{2}a} \mathrm{d}x\, \tau_o^2(x), \end{aligned}\right\} \tag{3.2}$$

and the prime denotes differentiation with respect to x.

When $\mu_s = 0$,
$$\mu^2 - 1 = 4[\tau_e \tau_e']^2 \frac{I_{ee}}{I_{oo}} = 4[\tau_o \tau_o']^2 \frac{I_{oo}}{I_{ee}}, \tag{3.3}$$

and this, together with the fact that the Wronskian of τ_e and τ_o is unity, makes it obvious from the band structure equation (2.12) that degeneracies of the Bloch waves can only occur at the Bragg orientations. Assuming that a particular choice of the relativistic factor γ will ensure that μ_n^2 is unity, reference to the labelling scheme of figure 3 and equation (2.12) shows that Bloch waves n and $n+1$ can only degenerate at some $s_c^{(n)}$, $\gamma_c^{(n)}$ when

$$\left.\begin{aligned} &\mu(s_c^{(n)}, \gamma_c^{(n)}) = \cos n\pi, \\ &\mu_s(s_c^{(n)}, \gamma_c^{(n)}) = 0, \\ &K_0 = K_0^B = (n + 2M)\,\pi/a \end{aligned}\right\} \tag{3.4}$$

(M is any integer). These conditions impose two constraints on μ and μ_s, so that if only s is varied the degeneracy is accidental. In electron microscopy, γ is also varied by altering the accelerating energy of the incident electrons, but over a limited range, so that only a few of these degeneracies can be obtained; they are known as *critical voltage effects*.

By differentiating (2.5) with respect to γ rather than s, it can be found by a similar analysis that at $(s_c^{(n)}, \gamma_c^{(n)})$ we must have

$$\left.\begin{aligned} &\mu_s = \mu_\gamma = 0, \\ &\mu_{ss} = -4\mu I_{ee} I_{oo}, \\ &\mu_{\gamma\gamma} = -4\mu U_{ee} U_{oo}, \\ &\mu_{s\gamma} = 2\mu[I_{oo} U_{ee} + I_{ee} U_{oo}], \end{aligned}\right\} \tag{3.5}$$

where as usual all the functions are evaluated at $\frac{1}{2}a$ and the new integrals are defined by

$$\left.\begin{aligned} U_{ee} &= \int_0^{\frac{1}{2}a} \mathrm{d}x\, \tau_e^2(x)\, \bar{U}_0(x), \\ U_{oo} &= \int_0^{\frac{1}{2}a} \mathrm{d}x\, \tau_o^2(x)\, \bar{U}_0(x) \end{aligned}\right\} \tag{3.6}$$

(remember that the potential $\bar{U}(x)$ has been written as $\gamma \bar{U}_0(x)$). In fact $\mu(s, \gamma)$ has a saddle point, or some higher stationary point, since at $(s_c^{(n)}, \gamma_c^{(n)})$ the discriminant is

$$\Delta \equiv \mu_{s\gamma}^2 - \mu_{ss}\mu_{\gamma\gamma} = 4\mu^2[I_{oo} U_{ee} - I_{ee} U_{oo}]^2 \geqslant 0. \tag{3.7}$$

We can now solve the band structure equation (2.12) near a degeneracy. For simplicity, we shall assume that the degeneracy is at an even Bragg orientation and that K_0 is near zero. (A similar analysis holds for a degeneracy at an odd Bragg position, and the results obtained near $K_0 = 0$ can always be related to the equivalent even Bragg positions using (2.16) and (2.17).) The band structure $s(K_0)$ is the (two-branched) hyperbola

$$(\tfrac{1}{2}K_0 a)^2 + (s - s_c)(\gamma - \gamma_c)(I_{oo} U_{ee} + I_{ee} U_{oo}) - (s - s_c)^2 I_{ee} I_{oo} = (\gamma - \gamma_c)^2 U_{ee} U_{oo}. \tag{3.8}$$

This becomes a degenerate line pair, so that the bands cross but do not touch, at the critical value $\gamma = \gamma_c$ (we shall occasionally denote $\gamma_c^{(n)}$ and $s_c^{(n)}$ by γ_c and s_c).

At $K_0 = 0$, denoting the branches of (3.8) which correspond to the even and odd Bloch waves as s_e and s_o respectively, we can show that the separation of the two bands represented by (3.8) is given by

$$\frac{s_e(0) - s_o(0)}{\gamma - \gamma_c} = \frac{U_{ee}}{I_{ee}} - \frac{U_{oo}}{I_{oo}}. \tag{3.9}$$

It is now clear that, unless the right hand side of (3.9) vanishes at $\gamma = \gamma_c$ (in which case $\Delta = 0$ and μ has a higher order stationary point), the symmetries of the Bloch waves n, $n+1$ which degenerate at (s_c, γ_c) must interchange as we pass through γ_c. Comparison with § 2 (*b*) thus shows that a higher order stationary point of μ corresponds to a zero of the reflexion coefficient R which is of higher order than unity. Finally, the right hand side of (3.9) is just the difference in the potential energies of the even and odd Bloch waves in the one dimensional potential $\bar{U}_0(x)$, so that the ordering of the symmetries of the Bloch waves above or below a known degeneracy tells us the sign of the relative potential energies of the waves in the projected potential.

(*a*) *The Bloch waves and their Fourier coefficients near a degeneracy*

In the last section, we indicated how the derivatives $\partial\tau_e/\partial s$, $\partial\tau_e/\partial\gamma$, etc., could be evaluated, and we may now expand the basis functions in Taylor series about (s_c, γ_c). Again we restrict our attention to a degeneracy at an even Bragg position, and use the equation for the branch of the band structure which has an odd solution at $K_0 = 0$; we find that, to lowest order,

$$\left.\begin{aligned} \tau_e(\tfrac{1}{2}a) &= \tau_e(\tfrac{1}{2}a\,; s_c, \gamma_c), \\ \tau_o(\tfrac{1}{2}a) &= \frac{\tau_e(\tfrac{1}{2}a)\,(\gamma - \gamma_c)\,\Delta^{\frac{1}{2}}}{4I_{ee}}\left[\sqrt{\left(1 + \frac{16(\tfrac{1}{2}K_0 a)^2 I_{ee} I_{oo}}{(\gamma - \gamma_c)^2 \Delta}\right)} - 1\right], \end{aligned}\right\} \tag{3.10}$$

where the functions and integrals on the right are evaluated at s_c, γ_c and we have chosen the branch

$$\Delta^{\frac{1}{2}} \equiv 2[I_{ee} U_{oo} - I_{oo} U_{ee}]. \tag{3.11}$$

It is now tedious but straightforward, to use (3.10) in (2.13), and the normalization of the Bloch waves, to determine the coefficients $A_o(K_0)$ and $B_o(K_0)$ in the expansion (2.11) of the Bloch wave $\tau_{oK_0}(x)$ for this 'odd branch' of the band structure (labelled henceforth by o). The general formulae are complicated, but two limits are relatively simple and illuminating.

First, let us suppose that $16(\tfrac{1}{2}K_0 a)^2 I_{ee} I_{oo} \ll (\gamma - \gamma_c)^2 \Delta$, which can always be achieved for small enough K_0 provided that $\gamma \neq \gamma_c$ and Δ does not vanish. It is found that

$$\left.\begin{aligned} A_o(K_0) &\approx \pm \frac{2I_{oo}(\tfrac{1}{2}K_0 a)}{(\gamma - \gamma_c)\,\Delta^{\frac{1}{2}}\sqrt{(2I_{oo})}}, \\ B_o(K_0) &\approx \pm\left(1 - 2(\tfrac{1}{2}K_0 a)^2 \frac{I_{oo} I_{ee}}{(\gamma - \gamma_c)^2 \Delta}\right)\Big/\sqrt{(2I_{oo})}, \end{aligned}\right\} \tag{3.12}$$

where the $\pm$ signs are to be taken together. We see that near γ_c, this Bloch wave which is odd at $K_0 = 0$, rapidly acquires an even component as K_0 is increased from zero. We shall see later that this has a pronounced effect on the Fourier coefficients $b_G^{(o)}(K_0)$ of this Bloch wave.

The second limit, when $16(\frac{1}{2}K_0a)^2 I_{ee}I_{oo} \gg (\gamma-\gamma_c)^2\Delta$, is relevant for larger tilts away from the exact Bragg position. We find that

$$\left.\begin{aligned} A_o(K_0) &\approx \pm\frac{1}{2\sqrt{I_{ee}}}\operatorname{sgn}(K_0\Delta^{\frac{1}{2}}(\gamma-\gamma_c)),\\ B_o(K_0) &\approx \pm\frac{1}{2\sqrt{I_{oo}}}, \end{aligned}\right\} \tag{3.13}$$

where sgn (x) is $+1$ if $x>0$ and -1 if $x<0$. These formulae show that the Bloch wave $\tau_{oK_0}(x)$ looks like a travelling wave in this region, rather than a standing wave as at $K_0=0$. Similar results are also obtained for the coefficients $A_e(K_0)$ and $B_e(K_0)$ of the Bloch wave $\tau_{eK_0}(x)$ corresponding to the even branch of the band structure (3.8). (In fact, they are the same as (3.12) and (3.13) with A_e and B_e instead of B_o and A_o respectively, o and e interchanged, and in the formulae for B_e the $\pm$ changed to $\mp$.) Finally, we note that the function sgn (x) above has not been defined for $x=0$. This is because formulae (3.13) do not apply if $K_0\Delta^{\frac{1}{2}}(\gamma-\gamma_c)$ is zero; either (3.12) must be used, or if $\gamma=\gamma_c$ we solve (3.8) afresh and find from (2.12) that for small $|K_0|\neq 0$

$$\frac{A}{B}=\pm\sqrt{\left(\frac{I_{oo}}{I_{ee}}\right)} \quad \text{if} \quad s-s_c=\pm\frac{(\frac{1}{2}K_0a)}{\sqrt{(I_{oo}I_{ee})}}. \tag{3.14}$$

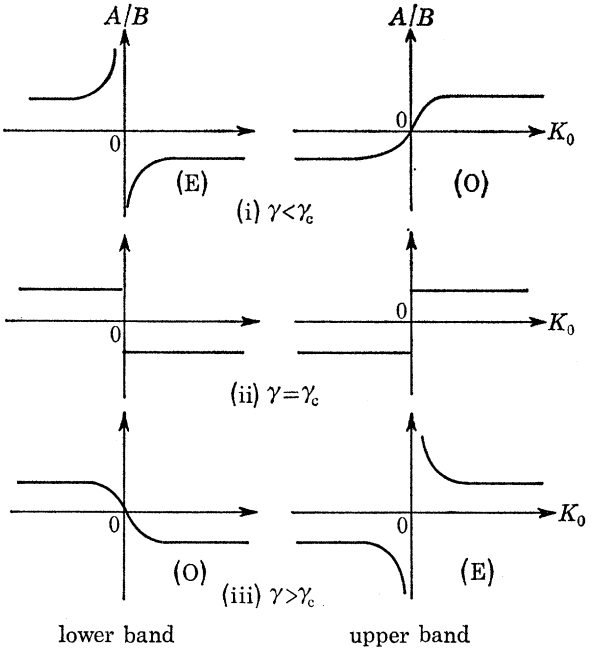

FIGURE 5. The ratio of the coefficients A/B is sketched as a function of γ and K_0 in the region of a degeneracy. The symmetries of the Bloch waves are as indicated by the letters E (for even) and O (for odd), assuming that $\Delta^{\frac{1}{2}}<0$.

At $K_0=0$ A and B are of course indeterminate. The variation of the ratio A/B predicted by equations (3.12)–(3.14) is sketched in figure 5, assuming that $\Delta^{\frac{1}{2}}<0$. The changes in the parities depicted there are consistent with the predictions of equation (3.9). If $\Delta^{\frac{1}{2}}$ were zero at (s_c, γ_c), then we should have to expand $\mu(s,\gamma)$, etc., to higher order. However, equation (3.9) shows that in this case the minimum separation of the bands at $K_0=0$ must vary at least as $(\gamma-\gamma_c)^2$, and our previous arguments about the phase of the reflexion coefficient show that it is possible to have

a degeneracy without an interchange of symmetry. Such a higher order degeneracy will occur only by chance ('accidentally') if we vary just γ, but we can also vary the shape of $\bar{U}(x)$ by changing the *temperature* and we shall see in § 5 that for some materials this is enough to produce such an effect.

We can of course easily substitute the expressions for the A, B coefficients above in the definition of the Fourier coefficients of the Bloch waves (2.8). Defining new integrals

$$\left.\begin{aligned} C_G^{1e} &\equiv \int_0^{\frac{1}{2}a} \mathrm{d}x\, \tau_e(x) \cos Gx, \\ S_G^{xe} &\equiv \int_0^{\frac{1}{2}a} \mathrm{d}x\, x\tau_e(x) \sin Gx, \end{aligned}\right\} \tag{3.15}$$

and similarly for S_G^{1o} and C_G^{xo}, we find, in the first limit above, that

$$\left.\begin{aligned} b_G^{(o)}(K_0) &= \pm\frac{1}{\sqrt{(\frac{1}{2}aI_{oo})}}\left\{\left(1-2(\tfrac{1}{2}K_0a)^2\frac{I_{ee}I_{oo}}{(\gamma-\gamma_c)^2\Delta}\right)S_G^{1o}+\frac{2(\frac{1}{2}K_0a)}{(\gamma-\gamma_c)\Delta^{\frac{1}{2}}}I_{oo}C_G^{1e}\right\}, \\ b_G^{(e)}(K_0) &= \pm\frac{1}{\sqrt{(\frac{1}{2}aI_{ee})}}\left\{\left(1-2(\tfrac{1}{2}K_0a)^2\frac{I_{ee}I_{oo}}{(\gamma-\gamma_c)^2\Delta}\right)C_G^{1e}-\frac{2(\frac{1}{2}K_0a)}{(\gamma-\gamma_c)\Delta^{\frac{1}{2}}}I_{ee}S_G^{1o}\right\}, \end{aligned}\right\} \tag{3.16}$$

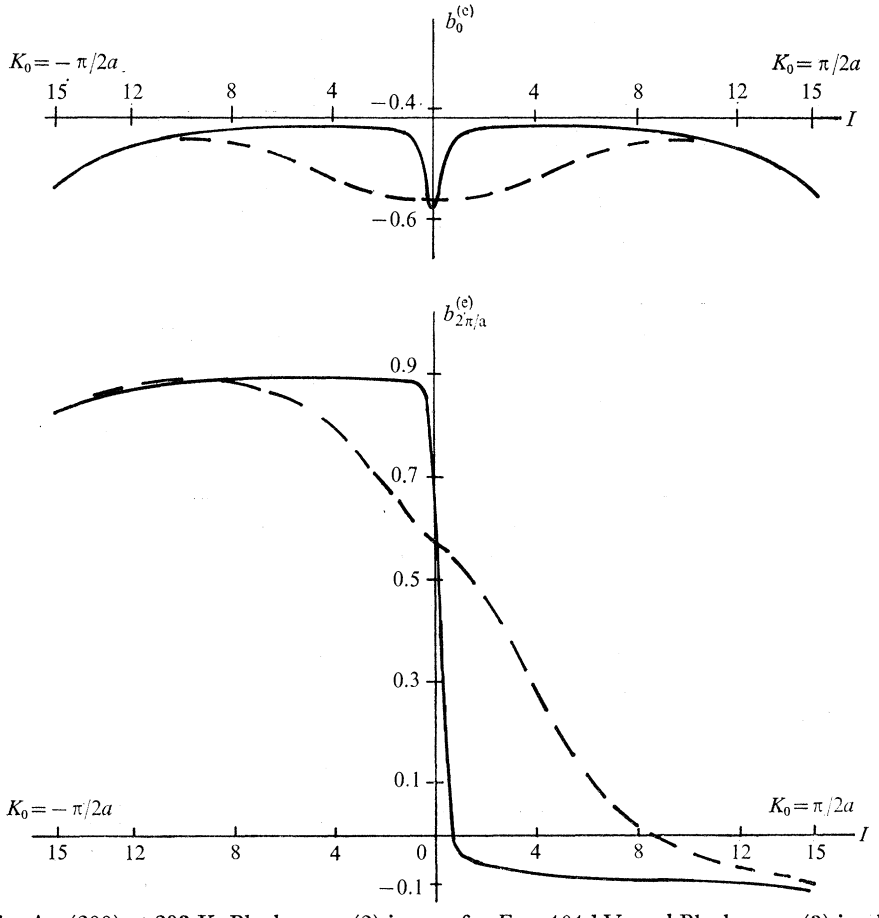

FIGURE 6. For Au (200) at 293 K, Bloch wave (2) is even for $E < 101$ kV, and Bloch wave (3) is odd. The Fourier coefficients $b_0^{(e)}$ and $b_{2\pi/a}^{(e)}$ of Bloch wave (2) are shown at 61 kV (------) and 100 kV (——). The orientation K_0 is given by $aK_0/2\pi = \pm 0.0028084\,(e^{0.3I}-1)$, so that the very rapid changes of $b_G^{(e)}(K_0)$ near $K_0 = 0$ can be seen. Even for $I = 5$, $K_0 = 0.009778 \times 2\pi/a$, showing that the K_0 scale is very nonlinear.

while in the second limit we have

$$\left.\begin{aligned} b_G^{(o)}(K_0) &= \pm\left\{\frac{S_G^{1o}+(\frac{1}{2}K_0a)\,C_G^{xo}}{\sqrt{(aI_{oo})}}+\operatorname{sgn}\left(K_0\Delta^{\frac{1}{2}}(\gamma-\gamma_c)\right)\left(\frac{C_G^{1e}-(\frac{1}{2}K_0a)\,S_G^{xe}}{\sqrt{(aI_{ee})}}\right)\right\},\\ b_G^{(e)}(K_0) &= \pm\left\{\frac{C_G^{1e}-(\frac{1}{2}K_0a)\,S_G^{xe}}{\sqrt{(aI_{ee})}}-\operatorname{sgn}\left(K_0\Delta^{\frac{1}{2}}(\gamma-\gamma_c)\right)\left(\frac{S_G^{1o}+(\frac{1}{2}K_0a)\,C_G^{xo}}{\sqrt{(aI_{oo})}}\right)\right\}.\end{aligned}\right\} \tag{3.17}$$

(Notice that S_0^{xe} and S_0^{1o} vanish identically.) All the qualitative features of equations (3.16) and (3.17) are shown by the calculated Fourier coefficients of Bloch waves 2 and 3 for gold (200) systematics at 293 K, which are displayed in figures 6 and 7. These Fourier coefficients were obtained directly by solving equations (2.10), truncated to a 17×17 matrix. In particular, we note the very rapid variation of the Fourier coefficients for γ near to γ_c, as predicted by equation (3.16).

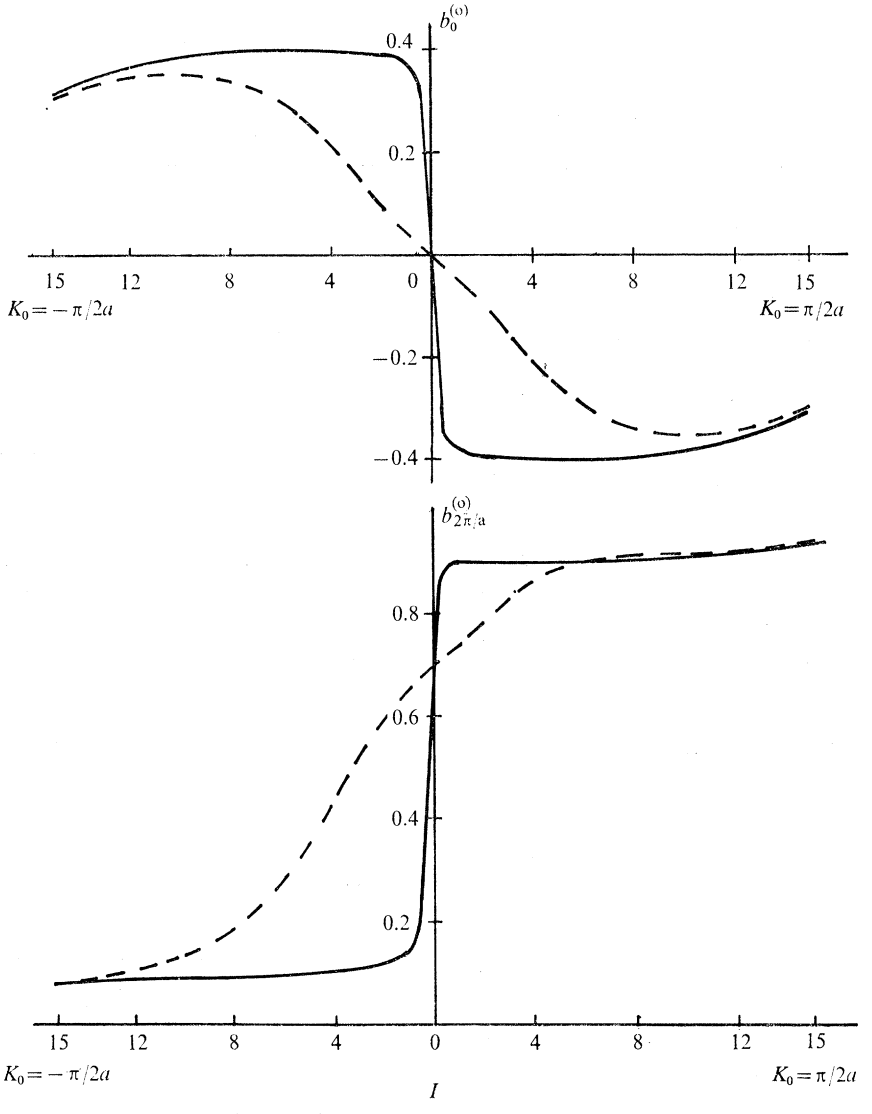

FIGURE 7. The Fourier coefficients $b_0^{(o)}$ and $b_{2\pi/a}^{(o)}$ are shown for 61 kV (------) and 100 kV (——) (the orientation K_0 is labelled in terms of the quantity I defined below figure 6).

(*b*) *Absorption effects near a degeneracy*

So far, we have regarded $V(\boldsymbol{r})$ and $\bar{U}(x)$ as real local potential energy functions. But this is not sufficient for a description of the elastic scattering of fast electrons by a crystal; Yoshioka (1957) showed that we must allow for some of the effects of the inelastic processes which take place in the crystal, in particular the reduction of the intensity of the elastically scattered waves. We can do this by adding to $\bar{U}(x)$ a small imaginary potential $\mathrm{i}\bar{U}^I(x)$, so that we have a complex 'optical potential' (optical potentials in diffraction theories are discussed in the review of Dederichs (1972)). Conventionally (Hirsch *et al.* 1965; Howie 1969), the small imaginary part of the potential, $\mathrm{i}\bar{U}^I(x)$, is included only by a first order non-degenerate perturbation calculation, so that the Bloch waves $\tau_{jK_0}(x)$ are unchanged to lowest order, but a small imaginary part is added to the eigenvalues $s_j(K_0)$. As pointed out by Sprague & Wilkins (1970) the form of the Bloch waves can be radically affected by this small perturbation, and we must perform a degenerate perturbation calculation near a critical voltage (Sheinin & Cann 1973). This is easily done for two Bloch waves $\tau_{nK_0}(x)$ and $\tau_{n'K_0}(x)$ which have unperturbed eigenvalues $s_n(K_0)$ and $s_{n'}(K_0)$ respectively ($s_n(0)$ and $s_{n'}(0)$ become equal at $\gamma = \gamma_c$). We find that the perturbed eigenvalues are

$$s_\pm = \tfrac{1}{2}\{s_n + s_{n'} + \mathrm{i}(\bar{U}^I_{nn} + \bar{U}^I_{n'n'}) \pm \sqrt{[(s_{n'} - s_n)^2 - (\bar{U}^I_{nn} - \bar{U}^I_{n'n'})^2 - 4|\bar{U}^I_{nn'}|^2 + 2\mathrm{i}(s_n - s_{n'})\,(\bar{U}^I_{nn} - \bar{U}^I_{n'n'})]}\}, \quad (3.18)$$

where $\bar{U}^I_{nn'}$ is a matrix element of $\bar{U}^I(x)$ between the states $\tau_{nK_0}(x')$ and $\tau_{n'K_0}(x)$.

Obviously, a long way from the Bragg orientation s_n and $s_{n'}$ are quite different and (3.18) may be expanded to give the usual non-degenerate result: for example, if $s_{n'} > s_n$,

$$s_+ = s_{n'} + \mathrm{i}\bar{U}^I_{n'n'} + \ldots. \quad (3.19)$$

However, $\bar{U}^I(x)$ is a symmetric potential if the real part $\bar{U}(x)$ of the potential is symmetric. Thus, very near a Bragg orientation, when the Bloch waves are to a good approximation purely even or odd functions of x (as indicated by equations (3.12) and in the sketches of figure 5), $|\bar{U}^I_{nn'}|$ is very small, and we find that (3.18) again reduces to (3.19). As shown by the calculations of Andrew & Sheinin (1974), the range of orientations for which the usual non-degenerate result (3.19) is valid is reduced as we approach γ_c, until when $\gamma = \gamma_c$ (3.19) is only correct for K_0 exactly equal to zero, when the degenerate Bloch waves may be chosen as even and odd. Our analytic expressions (3.12)–(3.14) also predict this behaviour.

Since $\bar{U}^I(x)$ is already diagonal with respect to the even or odd Bloch waves at a Bragg position, we can easily calculate to higher orders of perturbation theory. For instance, the second order contribution to s_e, namely

$$s_e^{(2)} = -\sum_{\substack{j \neq e \\ \epsilon_\delta^{(j)} = +1}} \frac{|\bar{U}^I_{je}|^2}{s_e - s_j} \quad (3.20)$$

is real, but extremely small because, as shown in figure 2, s_e is widely separated from all the other states of even parity. We shall see in the next section that it is most useful to define the critical voltage by the equality of the real parts of two of the eigenvalues s_j (the Bloch waves, labelled in order of increasing $\mathrm{Re}\, s_j$, then interchange their symmetries at the critical voltage), so that, if these second order contributions from $\bar{U}^I(x)$ are included, the critical voltage is slightly shifted (Lally *et al.* 1972). We shall ignore these very small contributions, and also very small corrections to the real part of the potential itself which are also due to inelastic processes (Yoshioka 1957).

(c) *The effect of a degeneracy on the diffracted waves and the Kikuchi pattern*

We have just seen that, at the Bragg position, we may use (2.9) for the diffracted wave amplitudes $A_G(K_0, z)$, provided absorption effects are included by adding a small imaginary part to the s_j. In the bright field ($G = 0$) case, we have (cf. equation (2.9))

$$A_0(K_0^{\mathrm{B}}, z) = \sum_{j \neq \mathrm{e,o}} (b_0^{(j)})^2 \exp\{-\mathrm{i}s_j z/2k_0\} + (b_0^{(\mathrm{e})})^2 \exp\{-\mathrm{i}s_{\mathrm{e}} z/2k_0\} + (b_0^{(\mathrm{o})})^2 \exp\{-\mathrm{i}s_{\mathrm{o}} z/2k_0\}, \quad (3.21)$$

where the contribution from the even and odd Bloch waves has been shown explicitly. At the critical voltage, $\mathrm{Re}\, s_{\mathrm{e}} = \mathrm{Re}\, s_{\mathrm{o}}$, so that the even and odd waves interfere *constructively*, and we should expect to see (besides the obvious increase of the extinction distance to infinity) a *maximum* in the bright field intensity $|A_0(K_0^{\mathrm{B}}, z)|^2$. The visibility of this maximum at the Bragg position will depend on the relative magnitudes of the $b_0^{(j)}$, the relative magnitudes of the $\mathrm{Im}\, s_j$ and also on the background intensity due to inelastic scattering. In § 4, we shall show that we may simultaneously choose $|b_0^{(\mathrm{e})}|$ and $|b_0^{(\mathrm{o})}|$ to be comparably large by a choice of K_0^{B}, and that $\mathrm{Im}\, s_{\mathrm{e}} \approx \mathrm{Im}\, s_{\mathrm{o}}$. Moreover, we shall show how the contributions from all the other Bloch waves may often be made small by the use of a thick crystal, so that this maximum intensity can be observed (Lally *et al.* 1972).

More dramatically, if we choose G to be $-2K_0^{\mathrm{B}}$, we can use the symmetry relation (2.20) to show that

$$A_{-2K_0^{\mathrm{B}}}(K_0^{\mathrm{B}}, z) = \sum_{j \neq \mathrm{e,o}} (b_0^{(j)})^2 \epsilon_s^{(j)}(K_0^{\mathrm{B}}) \exp\{-\mathrm{i}s_j z/2k_0\} + (b_0^{(\mathrm{e})})^2 \exp\{-\mathrm{i}s_{\mathrm{e}} z/2k_0\} - (b_0^{(\mathrm{o})})^2 \exp\{-\mathrm{i}s_{\mathrm{o}} z/2k_0\}, \quad (3.22)$$

so that the even and odd Bloch waves interfere *destructively*, and at $\gamma = \gamma_{\mathrm{c}}$ we expect the intensity $|A_{-2K_0^{\mathrm{B}}}(K_0^{\mathrm{B}}, z)|^2$ to be a *minimum*. If e and o stand for Bloch waves (2) and (3) and if $K_0^{\mathrm{B}} = 2\pi/a$, this is the 'disappearance of the second order line', often used to observe the degeneracy from bend contours (Nagata & Fukuhara 1967; Lally *et al.* 1972; Rocher & Jouffrey 1972).

However, most observations of the Bloch wave degeneracy are made from the Kikuchi pattern (Watanabe, Uyeda & Kogiso 1968; Watanabe, Uyeda & Fukuhara 1968; Thomas *et al.* 1973). According to the phenomenological theory of Thomas (1972), we may write the intensity in a direction K in the Kikuchi pattern from a crystal of thickness z as:

$$I(K, z) = \sum_G |A_G(K - G, z)|^2 \mathscr{F}(|K_0 - K + G|), \quad (3.23)$$

where K_0 indicates the direction of the incident electron beam, and $\mathscr{F}$ is a function which is fitted to the spread of the diffuse scatter about the incident direction. Since $\mathscr{F}$ decreases rapidly for large argument, Thomas approximates it by $\exp\{-a|K_0 - K + G|^b\}$. The validity of this expression, which was shown by Thomas to give a good description of the Kikuchi pattern for crystals of intermediate thicknesses, has been discussed by Høier (1973). Immediately, in the light of the last paragraph we can understand the disappearance of the second order Kikuchi line, since for $K_0 = 2\pi/a$ and $K = -2\pi/a$, the term $|A_{-4\pi/a}(2\pi/a, z)|^2$ dominates in the sum in (3.23).

Thomas (1972), however, points out that the reversal in the sense of asymmetry of the displaced Kikuchi line at $K = 0$ is probably a more sensitive indicator of the critical voltage. We can demonstrate analytically how this change is linked to the critical voltage. For $K_0 = 2\pi/a$ ($\equiv G_0$, say) and K small, the term $|A_{-G_0}(G_0, z)|^2$ gives the largest contribution to $I(K, z)$, so we neglect the other terms and also ignore in the dominant term all quantities having an oscillating thickness

dependence (because the Kikuchi pattern is not a sensitive function of thickness). For $\gamma \neq \gamma_c$, we eventually find, using the periodicity relation (2.16), that, if $s_j^I \equiv \operatorname{Im} s_j$,

$$I(K,z) \approx \sum_j [b_0^{(j)}(K)\, b_{G_0}^{(j)}(K)]^2\, \mathrm{e}^{-s_j^I(K)/k_0}\, \mathscr{F}(K), \tag{3.24}$$

an expression similar to that given by Høier (1972).

If $|K|$ is big enough it is easy to show from (3.17) that

$$(b_0^{(o)}(K)\, b_{G_0}^{(o)}(K))^2 = \frac{1}{a^2 I_{oo}^2}\left[(\tfrac{1}{2}Ka)\, C_0^{xo} + \operatorname{sgn}(\Delta^{\frac{1}{2}}K(\gamma-\gamma_c))\sqrt{\left(\frac{I_{oo}}{I_{ee}}\right)}\, C_0^{1e}\right]^2$$
$$\times\left[S_{G_0}^{1o} + (\tfrac{1}{2}Ka)\, C_{G_0}^{xo} + \operatorname{sgn}(\Delta^{\frac{1}{2}}K(\gamma-\gamma_c))\sqrt{\left(\frac{I_{oo}}{I_{ee}}\right)}\,(C_{G_0}^{1e} - (\tfrac{1}{2}Ka)\, S_{G_0}^{xe})\right]^2, \tag{3.25}$$

and that $(b_0^{(e)}(K)\, b_{G_0}^{(e)}(K))^2$ can be written in a similar form with $\operatorname{sgn}(\Delta^{\frac{1}{2}}K(\gamma-\gamma_c))$ replaced by $\operatorname{sgn}(\Delta^{\frac{1}{2}}K(\gamma_c-\gamma))$. The semiclassical expressions to be developed in § 4 will show that these terms are often the largest contribution to (3.24) and that $s_e^I \approx s_o^I$ (the other terms are in any case slowly varying over the range of K of interest). Thus, with the assumption that $\mathscr{F}(K)$ is also slowly varying we expect the Kikuchi pattern to be independent of the sign of $\gamma-\gamma_c$ in this region.

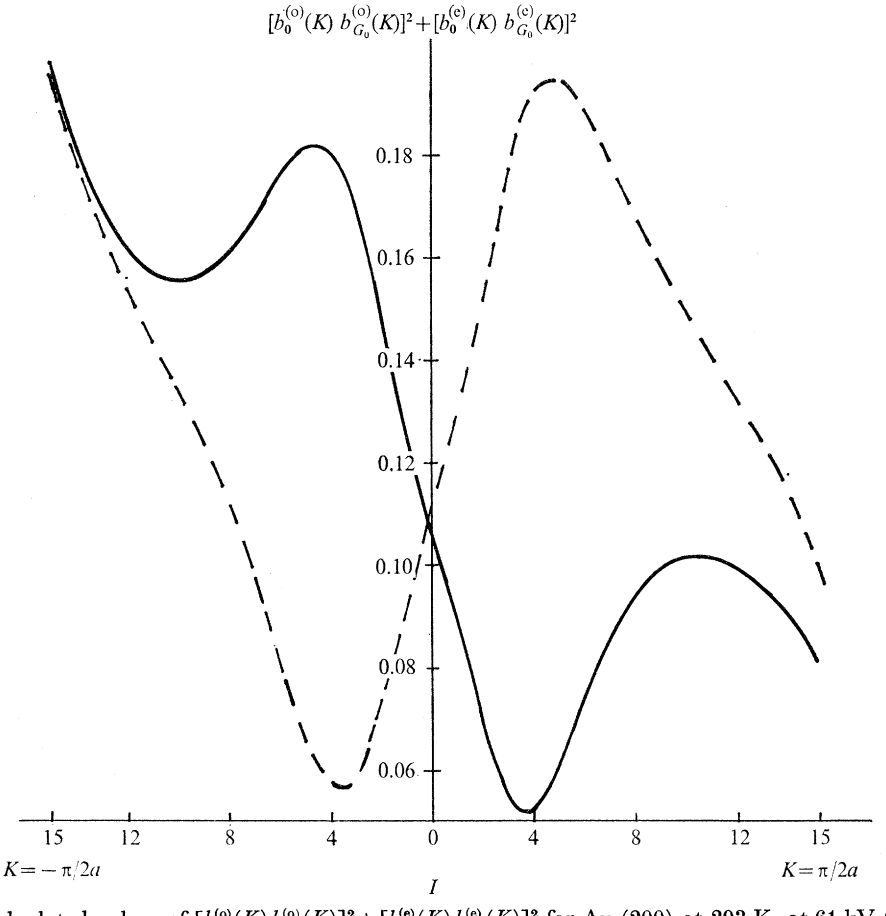

FIGURE 8. Calculated values of $[b_0^{(o)}(K)\, b_{G_0}^{(o)}(K)]^2 + [b_0^{(e)}(K)\, b_{G_0}^{(e)}(K)]^2$ for Au (200) at 293 K, at 61 kV (——) and at 141 kV (------) showing the reversal in asymmetry at $K = 0$. (The orientation K is labelled in terms of the quantity I defined below figure 6.)

For small K, we find to first order that:

$$(b_0^{(o)}(K)\, b_{G_0}^{(o)}(K))^2 + (b_0^{(e)}(K)\, b_{G_0}^{(e)}(K))^2 = \left(\frac{2C_0^{1e}}{aI_{ee}}\right)^2 \left[(C_{G_0}^{1e})^2 - \frac{4(\frac{1}{2}K_0 a)\, I_{ee} C_{G_0}^{1e} S_{G_0}^{1o}}{(\gamma-\gamma_c)\Delta^{\frac{1}{2}}}\right], \tag{3.26}$$

which, unlike (3.25) does depend on the sign of $\gamma-\gamma_c$. In particular (3.26) predicts that the slope at $K=0$ will change sign according as $\gamma \lesseqgtr \gamma_c$, a conclusion which is borne out by detailed calculation (figure 8) and explains the observed reversal in asymmetry of this Kikuchi line at the critical voltage.

4. Semiclassical approximations

It is not hard to use W.K.B. approximations for the transmission coefficient T to solve the band structure equations (2.12) and (2.15) (Berry 1971), and calculations based on these methods are in excellent agreement with exact 'many beam' calculations (Steeds & Enfield 1971; Berry *et al.* 1973), except near the Bragg positions and for states near the barrier top ($s_j \approx 0$). This is because the W.K.B. method only accounts for the waves reflected from the smooth top of a potential barrier and can never give transmission resonances. However, our scattering potentials have a discontinuity in curvature at $x = \pm\frac{1}{2}a$ as shown in figure 1, and this may give rise to reflected waves that interfere destructively with those reflected from the top of the barrier so that $|T|$ rises to unity (Berry *et al.* 1973). These effects are included in a formula for the modulus of the reflexion coefficient due to Landauer (1951)

$$|R| = \frac{1}{4}\left|\int_{-\frac{1}{2}a}^{\frac{1}{2}a} \mathrm{d}x \frac{\bar{U}'(x)}{s-\bar{U}(x)} \exp\left\{2\mathrm{i}\int_0^x \mathrm{d}x' \sqrt{(s-\bar{U}(x'))}\right\}\right|. \tag{4.1}$$

This may be obtained either by replacing the smooth scattering potential by a 'staircase' of tiny discontinuities and including waves reflected only once, or by iterating a pair of coupled integral equations which are equivalent to the Schrödinger equation (see, for example, Berry & Mount 1972). For the phase $\Phi(s,\gamma)$ defined in equation (2.15) we obtain the usual W.K.B. formula, which in the 'above-barrier' region, i.e. $s>0$, where (4.1) is valid, may be written as:

$$\Phi(s,\gamma) = \int_{-\frac{1}{2}a}^{\frac{1}{2}a} \mathrm{d}x \sqrt{(s-\bar{U}(x))}. \tag{4.2}$$

Similarly, we obtain W.K.B. expressions for the wave functions, so that we may write,

$$\left.\begin{aligned} \tau_e(x) &\approx \frac{\cos\left[\int_0^x \mathrm{d}x' \sqrt{(s-\bar{U}(x'))}\right]}{[s-\bar{U}(x)]^{\frac{1}{4}}} \equiv \frac{\cos(\phi(x))}{[s-\bar{U}(x)]^{\frac{1}{4}}}, \\ \tau_o(x) &\approx \frac{\sin\left[\int_0^x \mathrm{d}x' \sqrt{(s-\bar{U}(x'))}\right]}{[s-\bar{U}(x)]^{\frac{1}{4}}} \equiv \frac{\sin(\phi(x))}{[s-\bar{U}(x)]^{\frac{1}{4}}}, \end{aligned}\right\} \tag{4.3}$$

where we have introduced the 'incomplete phase' $\phi(x)$. These approximations are very useful in expressions involving integrals of the Bloch waves. For example, by using the standard method of stationary phase (Erdélyi 1956) as explained by Berry (1971), we may estimate the Fourier

coefficients $b_0^{(e,o)}(K_0^B)$ occurring in (3.21). Without loss of generality, suppose that $K_0^B > 0$; then, retaining only those integrals which include a stationary phase contribution, we find:

$$[b_0^{(e)}(K_0^B)]^2 \approx [b_0^{(o)}(K_0^B)]^2 \approx \frac{1}{a}\frac{\left[\int_0^{\frac{1}{2}a} \frac{dx}{[s-\bar{U}(x)]^{\frac{1}{4}}} \cos(\phi(x) - K_0^B x)\right]^2}{\int_0^{\frac{1}{2}a} \frac{dx}{\sqrt{[s-\bar{U}(x)]}}}. \tag{4.4}$$

Hence the excitations of the even and odd Bloch waves will be comparable at a critical voltage when $s = s_e = s_o = s_c$. It now remains to choose K_0^B so that these excitations are as large as possible. The phase is stationary at the classical turning point x_c, where

$$K_0^B = \sqrt{(s - \bar{U}(x_c))}, \tag{4.5}$$

so that, assuming $-\bar{U}'(x_c) > 0$ as is always the case for a simple potential like that shown in figure 1, the result of the approximate integration is

$$[b_0^{(e)}(K_0^B)]^2 \approx \frac{1}{a}\frac{[\sqrt{(4\pi/\bar{U}'(-x_c))}\cos(\phi(x_e) - K_0^B x_c + \frac{1}{4}\pi)]^2}{\int_0^{\frac{1}{2}a} \frac{dx}{\sqrt{[s-\bar{U}(x)]}}}. \tag{4.6}$$

The excitation will be largest when this stationary phase formula diverges most strongly, which happens when x_c is zero, since $\bar{U}'(0)$ vanishes by symmetry and the curvature of the potential is small there. However, $\bar{U}(0)$ is also zero so that we have, for the most favourable orientation

$$K_0^B \approx \sqrt{s_c}, \tag{4.7}$$

a result which remains valid even if there are several classical turning points in the range $[0, \frac{1}{2}a]$ and the potential has a more complicated form than that shown in figure 1. This crude estimate is shown later (§ 5 and figure 14) to be quite good in practice.

Moreover, even for $s < 0$, the semiclassical approximations in the classically accessible regions $(s - \bar{U}(x) > 0)$ have a form similar to equations (4.3), and equation (4.5) applies to all the even and all the odd Bloch waves, so that their excitations are only significant if (using (4.7))

$$\bar{U}(x_c^{(j)}) = s_j - s_c. \tag{4.8}$$

If K_c^2 is defined as the depth of the potential $\bar{U}(x)$, so that $-K_c^2 \leqslant \bar{U}(x) \leqslant 0$, we see from (4.8) that all the Bloch waves which contribute significantly to the diffracted wave amplitudes $A_G(K_0^B, z)$ lie in a region of width K_c^2 *below* s_c (Berry 1971). We shall see in a moment that provided s_c is the smallest positive eigenvalue the anomalous absorption effect can be used to ensure (by using a thick enough crystal) that only the degenerate Bloch waves contribute to the diffraction. For the special case $n = 2$ this was discovered by Lally *et al.* (1972).

(*a*) *Anomalous absorption effects*

The probability density of a bound (i.e. $s_j < 0$) state is large near the classical turning points, which in turn will be quite close to the projected atomic planes if the state is deeply bound. These states are therefore strongly inelastically scattered and their contribution to the diffracted waves emerging from a thick crystal is correspondingly small. Doyle & Berry (1973) found that for

a simple potential like that sketched in figure 1 the first order non-degenerate perturbation expression for s_j^I could be written as

$$s_j^I = \frac{\mathrm{Re}\int_0^{\frac{1}{2}a} \mathrm{d}x\, \bar{U}^I(x)/\sqrt{[s_j - \bar{U}(x)]}}{\mathrm{Re}\int_0^{\frac{1}{2}a} \mathrm{d}x/\sqrt{[s_j - \bar{U}(x)]}}, \tag{4.9}$$

a formula which is also valid for more complicated potentials if $s_j \geqslant 0$. They also showed that s_j^I has its minimum value at $s_j = 0$, so that Bloch waves with $|s_j|$ near zero are least absorbed, and bound states with large $|s_j|$ are strongly absorbed. Thus, if we have a degeneracy at s_c, and this is the smallest positive eigenvalue, and if the bound Bloch waves in our contributing 'band' below s_c do not lie near $s_j = 0$, a thick crystal can be used to ensure that the degenerate waves make the largest contributions to the diffraction.

Moreover, we see immediately from (4.9) that when $s_e = s_o = s_c$, s_e^I is equal to s_o^I so that the degenerate waves make comparable contributions to the diffraction; this gives rise to the effects discussed in § 3 (*c*).

(*b*) *The semiclassical formulae for a degeneracy*

In this section, it will be shown how the Landauer formula (4.1) may be used to predict many features of the critical voltage effect. Using the symmetry of the potential, we see from (4.1) that for a degeneracy of Bloch waves n and $n+1$ at (s_c, γ_c) we must have

$$\int_0^{\frac{1}{2}a} \mathrm{d}x\, \frac{\bar{U}'(-x)}{s_c - \bar{U}(x)} \sin\left\{2\int_0^x \mathrm{d}x'\sqrt{[s_c - \bar{U}(x')]}\right\} = 0, \tag{4.10}$$

while it is obvious from figure 2 by counting the eigensolutions of equation (2.26) that the phase Φ, given by equation (4.2), must also satisfy

$$\Phi = 2\int_0^{\frac{1}{2}a} \mathrm{d}x\sqrt{[s_c - \bar{U}(x)]} = n\pi. \tag{4.11}$$

To solve for s_c and γ_c we define a 'scaled' eigenenergy s_0 by

$$\gamma_c s_0 = s_c, \tag{4.12}$$

and recall that $\bar{U}(x)$ may be written as $\gamma\bar{U}_0(x)$ (cf. § 2 (*a*)), so that (4.10) and (4.11) become the relativistically scaled equations

$$\sqrt{\gamma_c} = \frac{n\pi}{2\int_0^{\frac{1}{2}a} \mathrm{d}x\sqrt{[s_0 - \bar{U}_0(x)]}} \tag{4.13}$$

and

$$\int_0^{\frac{1}{2}a} \mathrm{d}x\, \frac{\bar{U}_0'(-x)}{s_0 - \bar{U}_0(x)} \sin\left[\frac{n\pi\int_0^x \mathrm{d}x'\sqrt{[s_0 - \bar{U}_0(x')]}}{\int_0^{\frac{1}{2}a} \mathrm{d}x'\sqrt{[s_0 - \bar{U}_0(x')]}}\right] = 0. \tag{4.14}$$

These last two equations are extremely useful, both computationally (§ 5) and qualitatively.

As an example, let us suppose that the potential has the simple form sketched in figure 1 so that $\bar{U}_0(x)$ is a decreasing function of x in the range $[0, \frac{1}{2}a]$. If n is unity, then (4.14) is the integral of a positive semidefinite quantity and can only be zero if $\bar{U}_0'(x) = 0$ for all x (which is just the free electron case). Therefore degeneracies involving Bloch waves (1) and (2) will not occur for this

form of potential. For $n = 2$, the sine term in (4.14) changes sign once as x varies from 0 to $\frac{1}{2}a$, dividing the integrand into positive and negative portions. The prefactor $\bar{U}_0'(-x)/[s_0 - \bar{U}_0(x)]$ typically has the form shown in figure 9; thus if s_0 is correctly chosen, the integral can be made to vanish and a degeneracy will occur. If $n = 3$, the integrand has a negative portion in the middle of the range which often does not cancel the positive contributions from the ends for any choice of s_0 so that degeneracies of Bloch waves (3) and (4) often do not occur for this type of potential. For larger values of n, cancellation seems more likely and we can imagine degeneracies at more than one value of s_0 (and therefore at more than one γ_c) for a given n. For *very* large n, however, both repeated integration of (4.14) by parts (Erdélyi 1956), or an evaluation of the integral by contour methods (see, for example, Berry & Mount 1972) indicate that the integral behaves asymptotically as $\exp\{-\text{const} \times n\}$ and so is non-zero, showing that degeneracies do not then occur. Therefore, the total number of degeneracies for any smooth potential $\bar{U}_0(x)$ is finite. For the small values of n likely to be encountered in practice, we shall use the qualitative form of (4.13) and (4.14) to predict which Bloch waves can degenerate and to understand how γ_c varies with the temperature of the specimen. It is to this latter point that we now turn.

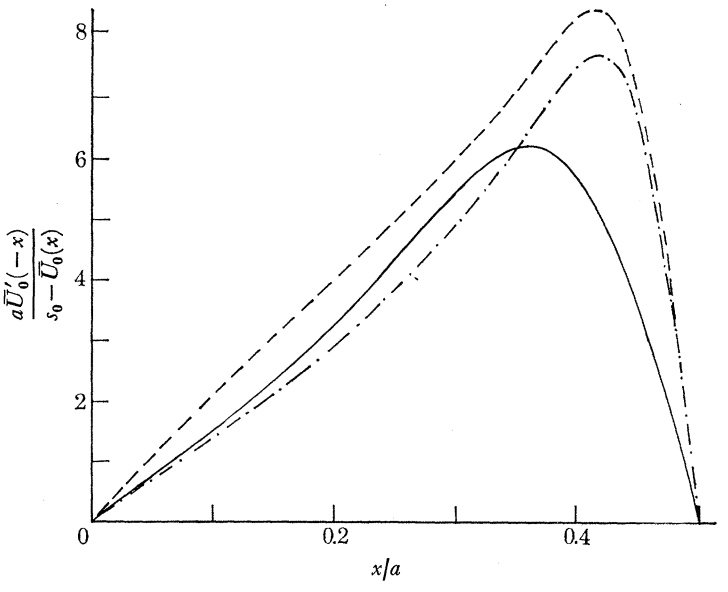

FIGURE 9. $a\bar{U}_0'(-x)/[s_0 - \bar{U}_0(x)]$ for Pb (200) systematics for (i) $s_0 = s_0^{(2)} = 3.022$; $W = 2.450$, i.e. 293 K (——); (ii) $s_0 = 3.022$; $W = 0.805$, i.e. 93 K (—·—); (iii) $s_0 = s_0^{(2)} = 1.944$; $W = 0.805$, i.e. 93 K (------).

(*c*) *The variation of critical voltage with temperature*

Temperature enters our theory through a Debye–Waller factor $\exp\{-M_{\kappa G}\}$ which is included in each of the Fourier coefficients V_G of the potential $\bar{V}(x)$ and accounts for the smoothing away by thermal motion of the discontinuities in the slope of $\bar{V}(x)$ arising from the Coulomb singularities in the atomic potentials at the nuclei. In the harmonic approximation $M_{\kappa G}$ is written as $W(G/4\pi)^2$ so that decreasing the temperature decreases W (see for instance the International Tables for X-ray Crystallography (1965)). The result is that the minima of the potential become deeper and sharper as shown in figure 10, basically because of the decreasing amplitude of thermal motion of the atoms. In turn this shifts the peak in the prefactor $\bar{U}_0'(-x)/[s_0 - \bar{U}_0(x)]$ towards $x = \frac{1}{2}a$ and increases the value of this factor in this region. The peak is also somewhat

narrower and the value of the factor is decreased in the neighbourhood of $x = 0$ (figure 9) because of a flattening of the potential near $x = 0$.

The effect of decreasing W is only very small as far as the phase integral $\int_0^x \mathrm{d}x' \sqrt{[s_0 - \bar{U}_0(x')]}$ is concerned, so the value of s_0 which gave a degeneracy at 293 K (say) will not give a degeneracy at 93 K (say). To make the integral in (4.14) zero at 93 K it is necessary to reduce s_0 so that the contribution from the neighbourhood of $x = 0$ is increased in comparison to that from the neighbourhood of $x = \frac{1}{2}a$ (figure 9). Equation (4.13) shows that γ_c will therefore be increased. This is indeed found to happen (see for instance the results given in § 5) for any n in the range 2–6; the exception occurs when two degeneracies occur for the same n but slightly differing s_0 (see § 5), and it is to a discussion of this case that we now turn.

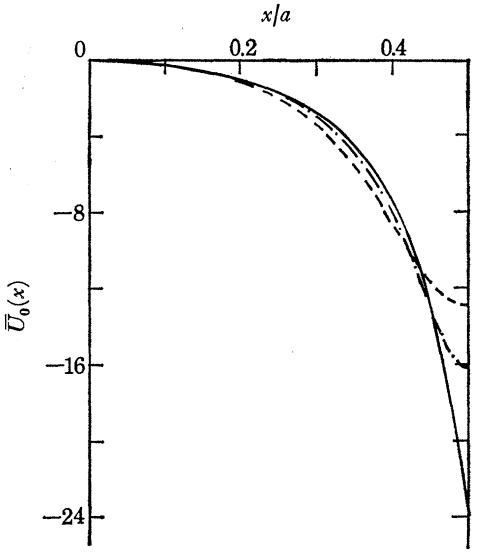

FIGURE 10. (200) systematic potentials of lead at (i) 293 K, $W = 2.450$ (------); (ii) 93 K, $W = 0.805$ (—·—); (iii) static lattice $W = 0$ (——). For $W \neq 0$ the Fourier series (2.3) is rapidly convergent. For $W = 0$ the series converges only slowly, and Kummer's method of summation (Abramowitz & Stegun 1964, p. 16) was used, with $V_G \to \text{const}/(G^2 + b)$ as $G \to \infty$.

(*d*) *The occurrence of critical voltages for symmetric potentials*

We shall now discuss how two degeneracies can occur for a given value of n, and also whether a given degeneracy can occur for a given symmetric potential (general asymmetric potentials are dealt with in the appendix). To be concrete let us consider the case of Pb (200) systematics. At low temperatures W is 0.805, a value similar to the values taken by the Debye–Waller parameters of most other metals at room temperature. For $n = 3$, the factor $\bar{U}_0'(-x)/[s_0 - \bar{U}_0(x)]$ is quite sharply peaked at this temperature (figure 11), and as discussed in § 4 (*b*) there is no degeneracy. As we increase the temperature, figure 11 shows that the peak broadens, until suddenly, at $W = 1.536$, there appears a pair of values of s_0 which cause the integral to vanish, and there are two critical voltages for a degeneracy of Bloch waves (3) and (4) which persist at higher temperatures. We shall see in § 5 that this sudden appearance of two critical voltages is a higher order degeneracy (§ 3). Qualitatively, we can say that degeneracies of Bloch waves (3) and (4) will only occur for potentials of the form shown in figure 1 if the Debye–Waller

parameter W is large enough. Such degeneracies are expected to occur in pairs, approaching, coalescing and disappearing as the temperature is reduced.

As a final example, let us consider a more complicated form of the potential, for instance the (111) systematic potential of silicon. This potential is sketched in figure 12*a* together with the form of the factor $\bar{U}_0'(-x)/[s_0-\bar{U}_0(x)]$ in figure 12*b*. The (111) planes of the diamond structure occur in pairs so that there are two different potential barriers between neighbouring planes of

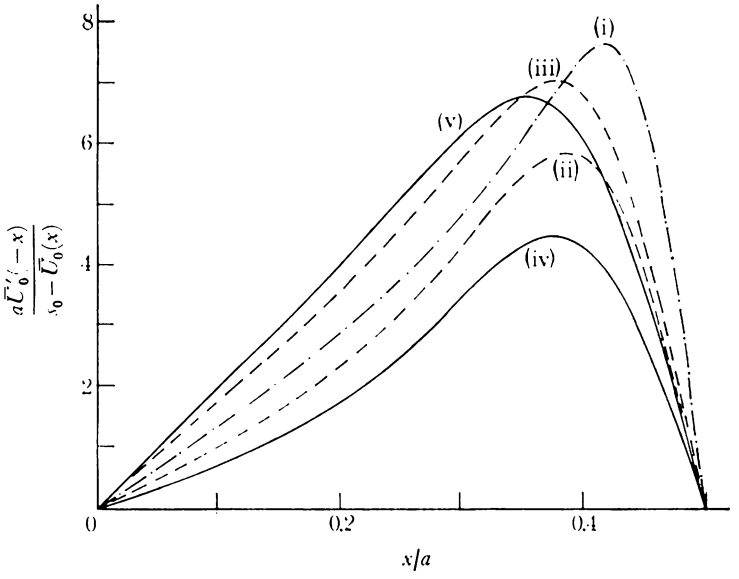

FIGURE 11. $a\bar{U}_0'(-x)/[s_0-\bar{U}_0(x)]$ for Pb (200) systematics for: (i) $W = 0.805$, $s_0 = 3.1$ (—·—); (ii) $W = 1.75$, $s_0 = s_0^{(3,1)} = 4.404$ (------); (iii) $W = 1.75$, $s_0 = s_0^{(3,2)} = 2.466$ (------); (iv) $W = 2.45$, $s_0 = s_0^{(3,1)} = 6.638$ (——), (v) $W = 2.45$, $s_0 = s_0^{(3,2)} = 2.235$ (——).

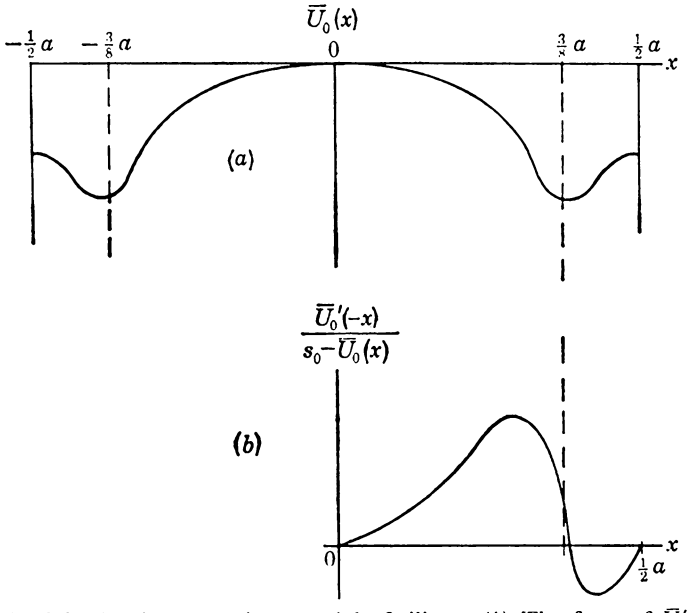

FIGURE 12. (*a*) A sketch of the (111) systematic potential of silicon. (*b*) The form of $\bar{U}_0'(-x)/[s_0-\bar{U}_0(x)]$. Note that the minimum of $\bar{U}_0(x)$ occurs for x just greater than $3a/8$ (where there is a (111) plane of atoms).

atoms. Because of the zero of $\bar{U}_0(-x)$ near $x = 3a/8$ we can readily understand from the integral in (4.14) why Bloch waves (2) and (3) do not degenerate for this potential, whereas waves (3) and (4) do.

5. Calculation of critical voltages

It was very easy to solve equations (4.14) and (4.13) by numerical integration on a computer so that from equation (2.2) a quick estimate of the critical voltage $E_c^{(n)}$ at which Bloch waves n and $n+1$ degenerate was obtained. The potential $\bar{U}_0(x)$ and its derivative $\bar{U}_0'(x)$ were obtained by summing their Fourier series, using the free atom form factors given by Doyle & Turner (1968) and a mean of the values of the Debye–Waller parameters W given in the International Tables for X-ray crystallography to calculate the Fourier coefficients V_G (see, for example, Howie 1969). For small values of $G/4\pi$ (generally $G/4\pi < 6\,\text{Å}^{-1}$) the form factors were obtained by interpolation from the tables given by Doyle & Turner, but for larger values, a screened Coulomb form

$$f_{el}\left(\frac{G}{4\pi}\right) = \frac{m_0 Ze^2}{2h^2}\,\frac{1}{b+(G/4\pi)^2} \tag{5.1}$$

Table 1. A comparison of the values obtained (kV) for the critical voltages of light, medium and heavy elements, as calculated from the Landauer formula for $|R(s)|$ and 'exact' 'many-beam' matrix calculations

			293 K			93 K		
element	reflexion	n	W	$E_c^{(n)}$ matrix	$E_c^{(n)}$ Landauer	W	$E_c^{(n)}$ matrix	$E_c^{(n)}$ Landauer
Al	(111)	2	0.820	474	450	0.355	550	520
		4		3037	3023		3803	3773
		6		4475	4493		9104	9076
Cu	(200)	2	0.530	687	644	0.210	802	745
		4		4171	4135		5215	5141
		6		7385	7378		10230	10197
Mo	(110)	2	0.255	74	51	0.105	93	68
		4		2107	2076		2294	2256
		6		5082	5056		5910	5866
Au	(200)	2	0.590	101	76	0.200	164	131
		4		1752	1739		2322	2286
		5		1638	1651		—	—
		5		3698	3656		—	—
		6		1380	1373		5900	5834

was fitted to join continuously at the largest tabulated value of $G/4\pi$. We also solved a truncated set of 'many-beam' equations (2.10) at the appropriate Bragg position for several values of γ near the semiclassical estimate and used the abrupt change in parity of the eigenvectors $\{b_G^{(j)}(K_0^B)\}$ to obtain voltages above and below $E_c^{(n)}$. Linear interpolation from these voltages gave an 'exact' $E_c^{(n)}$, the accuracy of which was checked by increasing the size of the array of many-beam equations and repeating the process. Usually a 17×17 or 16×16 array of equations was sufficient to give $E_c^{(n)}$ to an accuracy of 1 kV or better.

At most only the first six or seven Bloch waves contribute to the diffracted beams used in electron microscopy, so the calculations were restricted to these. Table 1 shows the results for elements of low, medium and high atomic number. All the systematic potentials corresponding to the results given in table 1 are similar to the potential sketched in figure 1 and degeneracies of

the same pairs of Bloch waves are possible in each case. However, only Au (200) exhibits a degeneracy of waves (5) and (6) at an odd Bragg position, and it has two such degeneracies at 293 K, but none at 93 K! One of these degeneracies occurs at a high voltage when s_c is small compared to K_c^2 and the other at the lower voltage when s_c is much larger. Au (111) has a similar pair of degeneracies, but this behaviour is not restricted to heavy elements since Al (200) behaves similarly.

TABLE 2. SOME CRITICAL VOLTAGES (kV) OF CADMIUM (*a*) AT 293 K AND (*b*) AT 86 K, AND OF LEAD (*a*) AT 293 K AND (*b*) AT 93 K

			(*a*)			(*b*)		
element	reflexion	n	W	$E_c^{(n)}$ matrix	$E_c^{(n)}$ Landauer	W	$E_c^{(n)}$ matrix	$E_c^{(n)}$ Landauer
Cd	(0002)	3	2.610	25	22	0.800	—	—
		3		574	545		—	—
		4		35	35		1405	1385
		5		0.1	0.62		—	—
		5		1251	1243		—	—
		6		1312	1306		2123	2140
		6		2926	2907		—	—
Pb	(111)	3	2.450	99	96	0.805	—	—
		3		521	490		—	—
		4		129	129		1292	1279
		5		90	91		1671	1693
		5		1676	1672		2516	2468
		6		9	9		1260	1270
		6		1667	1661		—	—
		6		3561	3535		—	—
Pb	(200)	2	2.450	20	5	0.805	159	128
		3		218	216		—	—
		3		864	832		—	—
		4		212	212		1781	1774
		5		120	121		1946	1964
		5		2012	2005		3688	3638
		6		1948	1942		1780	1787
		6		4630	4607		—	—

Elements with larger values of the Debye–Waller parameter W exhibit a much greater variety of degeneracies. Lead and cadmium have exceptionally large values of W at room temperature, although W is much smaller at low temperatures since these elements have small Debye temperatures. Table 2 shows the degeneracies found amongst the first seven Bloch waves for some of the simple potentials of these elements. It is notable that for Cd (0002) and Pb (111) no degeneracy of Bloch waves (2) and (3) appears in the table. Even when the beam voltage is reduced to zero, wave (2) remains odd, so the critical value of γ, below which wave (2) would be even, is less than unity and hence physically inaccessible. For Au (111) at 293 K, Bloch wave (2) is similarly odd at $\gamma = 1$. These potentials are all strong so that the lowest Bloch wave is deeply bound within the potential well at the atomic planes, and the first resonance maximum of $|T(s)|$ is above the second maximum of $\cos\Phi$ as in figure 3 (*c*).

From tables 1 and 2 we see that our formulae can be used to provide rather accurate estimates of the critical voltages, even though these depend quite sensitively on the detailed shape of $\bar{U}_0(x)$. Indeed, as table 3 shows they are no less accurate when used to predict the critical voltages of the more complicated (111) systematic potential of silicon. As discussed in § 4 (*d*), there is no

degeneracy of Bloch waves (2) and (3) for this potential, and the first degeneracy at an even Bragg position is between waves (6) and (7). For all the degeneracies we have studied, the values of γ_c found from the semiclassical formulae have been accurate to within about 4 %, and frequently to within 2 % or better. Figure 13 shows that the formulae give more accurate results for the larger values of s_c. This is because the W.K.B. approximation for the phase is an asymptotic formula, valid for large actions; i.e. it is a good approximation for large s; in the same limit the Landauer formula should accurately predict the zeros of R, since it has been shown that the asymptotic form of the Landauer formula is proportional to the asymptotic form of $|R|$ (see for example, Berry & Mount 1972, Pokrovskii, Ulinich & Savvinykh 1958).

TABLE 3. CRITICAL VOLTAGES (kV) OF SILICON (111) AT 293 K AND 93 K

(The atomic form factors for G = (111), (333), (444) and (555), and the Debye–Waller parameters, were taken from the X-ray measurements of Aldred (1971). All other scattering factors were obtained in the usual way from the table given by Doyle & Turner (1968).)

			293 K			93 K		
element	reflexion	n	W	$E_c^{(n)}$ matrix	$E_c^{(n)}$ Landauer	W	$E_c^{(n)}$ matrix	$E_c^{(n)}$ Landauer
Si	(111)	3	0.4615	1145	1109	0.2274	1200	1160
		5		1594	1595		1625	1625
		6		5825	5794		6279	6238

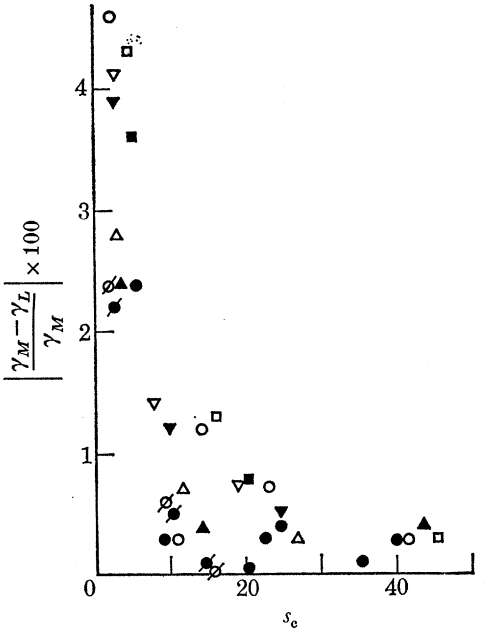

FIGURE 13. The relative accuracy of the critical voltages predicted by the semiclassical formulae, plotted against s_c at 293 K (solid symbols) and at 93 K (open symbols), according to the scheme: ●, Pb (200); ■, Cu (200); ▲, Al (111); ▼, Mo (110); ◪, Si (111).

Finally, we note that it was also possible to inspect the eigenvectors of the 'many-beam' calculations to obtain the orientations at which $[b^{(e,o)}(K_0^B)]^2$ were large. These orientations are shown plotted against $a\sqrt{(s_c)}/2\pi$, the prediction of equation (4.7), in figure 14. For the examples studied here, it turned out that

$$\sqrt{s_c} < K_0^B < \sqrt{s_c} + 2\pi/a. \tag{5.2}$$

The lower bound is easily understood: we deduced (4.7) by letting $x_c \to 0$ in (4.6) but the fact that $-\bar{U}(x_c) \geqslant 0$ implies that we should have $\sqrt{s_c} \leqslant K_0^B$. The upper bound in (5.2) shows that this extremely crude estimate is not too bad.

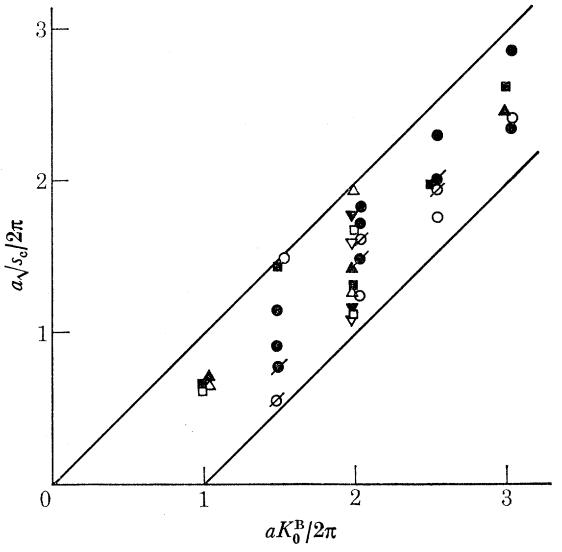

FIGURE 14. $a\sqrt{s_c}/2\pi$ is plotted against the orientations $aK_0^B/2\pi$ described in the text; the solid symbols refer to calculations at 293 K, and the open symbols to calculations at 93 K, as follows: ●, Pb (111); ■, Au (200); ▲, Al (111); ▼, Mo (110); ◆, Si (111).

(*a*) *Higher order degeneracies*

In tables 1 and 2 there are a number of critical voltages of the higher Bloch waves of gold, cadmium and lead which occur at 293 K but do not exist at 93 K. By repeating the calculations based on the semiclassical formulae for successively smaller values of the Debye–Waller parameter W, the variation of these critical voltages with temperature was followed (figure 15). We see that, as discussed in § 4 (*d*), a pair of critical voltages can indeed approach, coalesce and disappear as the temperature is reduced. However, it is easy to go further and show, by extending the methods used in § 3 to account for parameters other than γ, that as we vary the Debye–Waller parameter W the critical voltage moves along a trajectory $\gamma_c(W)$, determined by

$$\frac{1}{\gamma_c}\frac{\partial \gamma_c}{\partial W} = -\frac{U_{ee}^W(W)/I_{ee}(W) - U_{oo}^W(W)/I_{oo}(W)}{U_{ee}(W)/I_{ee}(W) - U_{oo}(W)/I_{oo}(W)}, \tag{5.3}$$

where

$$U_{ee}^W(W) \equiv \int_0^{\frac{1}{2}a} \mathrm{d}x \frac{\partial \bar{U}_0(W,x)}{\partial W} \tau_e^2(x), \quad \text{etc.} \tag{5.4}$$

The curves shown in figure 15 can be explained in terms of the smooth variation of the expressions in the numerator and denominator of equation (5.3). In particular, when the denominator is zero, $\partial\gamma_c/\partial W$ is infinite, as for example at $W \approx 0.60$ for Bloch waves (5) and (6) of Pb (200) (figure 15). At this point, there is a higher order degeneracy (see § 3) at which the Bloch waves degenerate *but do not interchange their parities* as γ is varied through γ_c. In this way, we can pass smoothly from a region where there are two critical voltages to a region where there are none, since whenever we *cross* the critical trajectory the parities of the Bloch waves are interchanged. It should be realized, however, that the higher order degeneracy can occur whenever we vary

γ *and* W along a tangent to the trajectory. This is easy to visualize from a plot of the surfaces of $\mu^2 = 1$ in the s, γ, W space. For the example of Bloch waves (5) and (6) of Pb (200), the two relevant surfaces are sketched in figure 16. Degeneracies occur whenever these surfaces cross, i.e. around the edge of the 'pocket'.

As yet none of these higher order degeneracies has been observed; indeed even the degeneracy of Bloch waves (3) and (4) for Pb (200), which occurs twice for voltages below 1000 kV, has not been observed, although Jones and Tapetado (1973) have observed a degeneracy of waves (3) and (4) for Cd (0002) at room temperature near 574 kV.

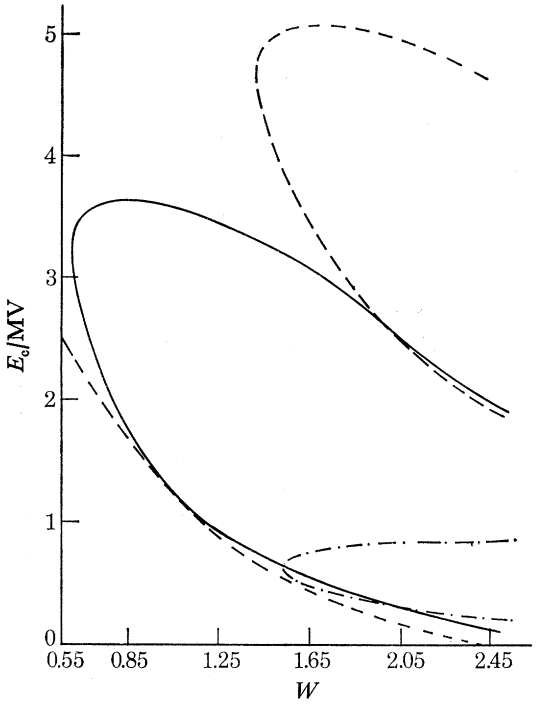

FIGURE 15. Some of the critical voltages of Pb (200) are plotted as functions of the Debye–Waller parameter W: $E_c^{(3)}$, —·—·—; $E_c^{(5)}$, ——; $E_c^{(6)}$, ------. These critical voltages were calculated from the semiclassical formulae.

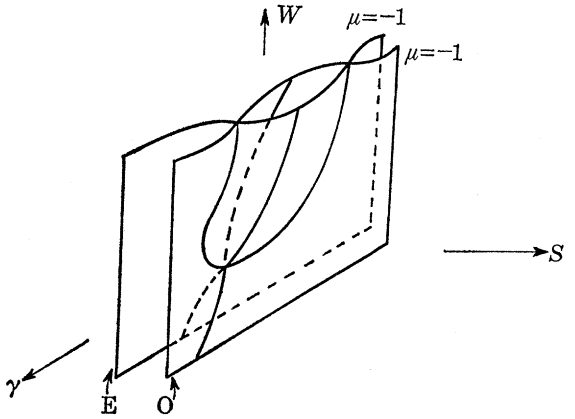

FIGURE 16. A sketch of the surfaces of $\mu(s, \gamma, W) = -1$ for Bloch waves (5) and (6) of Pb (200). The surface labelled E is associated with a symmetric solution of the Schrödinger equation and that labelled O with an antisymmetric solution.

We also estimated the lowest temperatures at which these trajectories exist by using a Debye model, for which

$$W = \frac{6h^2}{Mk_B\Theta}\left[\frac{\phi(\Theta/T)}{\Theta/T} + \frac{1}{4}\right], \tag{5.5}$$

where ϕ is the Debye function (see for instance the International Tables for X-ray Crystallography). Table 4 lists some of these temperatures, calculated not only from the semiclassical predictions of $E_c^{(n)}$, but also from the exact 'many-beam' critical voltages. The close agreement of these results shows again how accurate the semiclassical formulae are. In fact, we also calculated the critical voltages as a function of W by the 'many-beam' method, using equation (3.9) to calculate $\partial/\partial\gamma(s_e(0) - s_0(0))$ and Newton's famous algorithm to speed up the computations. The results given in figure 17 show that as usual the predictions of the semiclassical formulae were in good agreement with the exact calculations.

TABLE 4. A COMPARISON OF THE MINIMUM VALUES OF W AS OBTAINED FROM THE SEMICLASSICAL FORMULAE, AND FROM 'MANY-BEAM' CALCULATIONS

(The temperature $T_{\min}$ corresponding to the latter is given in the last column.)

				$W_{\min}$		
element	reflexion	Θ	n	Landauer	'many-beam'	$T_{\min}$/K
Au	(200)	168.5	5	0.311	0.305	143
Pb	(111)	82.0	3	1.713	1.66	200
			5	0.715	0.703	82
			6	1.603	1.59	192.9
Pb	(200)	82.0	3	1.535	1.49	180
			5	0.602	0.558	65
			6	1.415	1.41	169
Cd	(0002)	107.4	3	1.259	1.23	140
			6	1.797	1.79	201

6. RECONSTRUCTION OF THE POTENTIAL

The sensitivity of critical voltages to the form of the potential $\bar{U}(x)$ was first used to determine the lowest Fourier coefficient $U_{2\pi/a}$ (Watanabe *et al.* 1968) and has more recently been used to determine the atomic form factors $f_{el}(G/4\pi)$ and Debye temperatures (see, for example, Thomas *et al.* 1973; Shirley *et al.* 1975). The basis of these methods is the use of calculated values of the form factors for free atoms (e.g. those of Doyle & Turner 1968) as a good approximation to the form factors of atoms bound in a crystal for the larger values of $(G/4\pi)$. We, however, shall use the simple analytic forms of our semiclassical formulae to devise an inversion technique to obtain $\bar{U}(x)$ *directly* from the critical voltages $E_c^{(n)}$ (Buxton & Berry 1973; Berry *et al.* 1973).

We introduce the new variable

$$\psi(x) = \frac{2\sqrt{\gamma_c^{(n)}}}{n}\int_0^x \mathrm{d}x'\sqrt{[s_0 - \bar{U}_0(x')]}; \tag{6.1}$$

equation (4.14) may then be written in the form:

$$\int_0^\pi \mathrm{d}\psi f_n(\psi)\sin n\psi = 0, \tag{6.2}$$

where

$$f_n(\psi) = \frac{n}{2\sqrt{\gamma_c^{(n)}}}\frac{\bar{U}_0'(-x(\psi))}{[s_0 - \bar{U}_0(x(\psi))]^{\frac{1}{2}}} = -2\frac{\mathrm{d}}{\mathrm{d}\psi}\ln\left(\frac{\mathrm{d}x}{\mathrm{d}\psi}\right). \tag{6.3}$$

This last equation can be integrated to obtain exact formulae giving $\bar{U}_0(x)$ parametrically in terms of $f_n(\psi)$, namely

$$\bar{U}_0(x) = \frac{1}{\gamma_c^{(n)}}\left[\frac{n}{a}\int_0^{\pi} d\psi \exp\left\{-\frac{1}{2}\int_0^{\psi'} d\psi'' f_n(\psi'')\right\}\right]^2 \left(1-\exp\left\{\int_0^{\psi} d\psi' f_n(\psi')\right\}\right), \tag{6.4}$$

and

$$\frac{x}{a} = \frac{1}{2}\left(\frac{\int_0^{\psi} d\psi' \exp\left(-\frac{1}{2}\int_0^{\psi'} d\psi'' f_n(\psi'')\right)}{\int_0^{\pi} d\psi' \exp\left(-\frac{1}{2}\int_0^{\psi'} d\psi'' f_n(\psi'')\right)}\right). \tag{6.5}$$

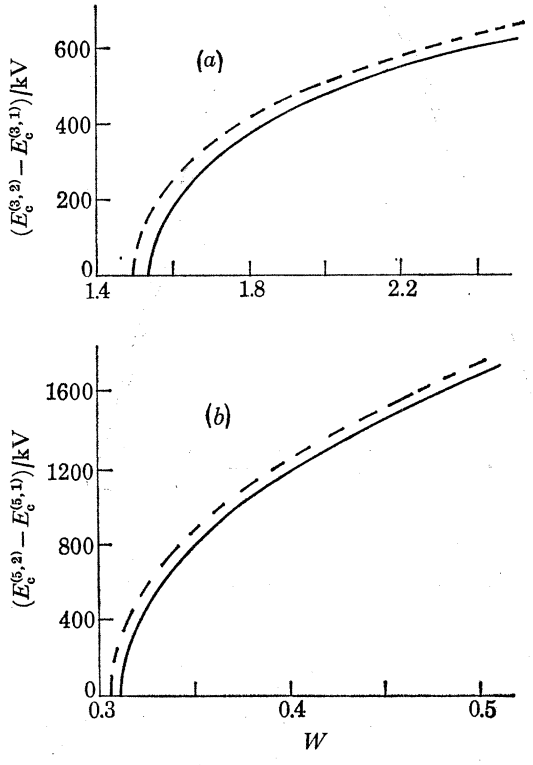

FIGURE 17. A comparison of pairs of critical voltages as calculated from the semiclassical formulae (——) and 'many beam' equations (------). (*a*) $E_c^{(3,2)} - E_c^{(3,1)}$ for Pb (200); (*b*) $E_c^{(5,2)} - E_c^{(5,1)}$ for Au (200).

Thus if we knew $f_n(\psi)$ at the value of s_0 appropriate to the degeneracy of Bloch waves n and $n+1$ we could calculate $\bar{U}_0(x)$. We shall approximate $f_n(\psi)$ by truncating its Fourier expansion; this may be written as

$$f_n(\psi) = \sum_{m=1}^{\infty} A_{nm} \sin(m\psi) \tag{6.6}$$

since $f_n(\psi)$ is an odd function. At the critical voltage, A_{nn} vanishes, but if we are to truncate the series we need to know that the neglected coefficients are small. It turns out that since the potential $\bar{U}_0(x)$ is an analytic function over the entire finite x plane, the only singularities of $f_n(\psi)$ in the finite ψ plane are simple poles due to the complex classical turning points x_i, at which $s_0 - \bar{U}_0(x_i)$ is zero. $f_n(\psi)$ is, therefore, analytic in a strip about the real ψ axis out to the nearest turning points, for which

$$|\operatorname{Im}\psi| \equiv \psi_i = \frac{2\sqrt{\gamma_c^{(n)}}}{n}\left|\operatorname{Im}\int_0^{x_i} dx\sqrt{[s_0 - \bar{U}(x)]}\right|. \tag{6.7}$$

The Fourier series (6.6) converges uniformly to $f_n(\psi)$ in this strip, so that, as shown by evaluating the coefficients A_{nm} by contour integration for large m (see, for example, Berry & Mount 1972), the A_{nm} decay exponentially, i.e.

$$A_{nm} \underset{m\to\infty}{\sim} \mathrm{e}^{-m\psi_i} \tag{6.8}$$

and we may hope that a truncation of (6.6) would be successful.

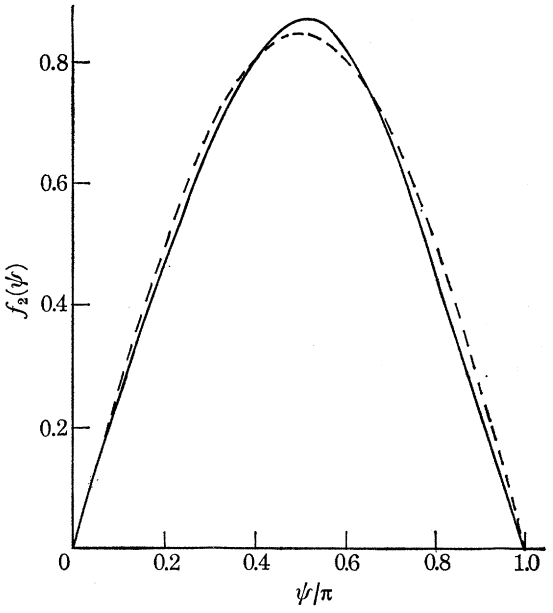

FIGURE 18. A comparison of $f_2(\psi)$ as calculated from equation (6.3) for Pb (200) at 293 K for $s_0 = 3.022$ Å^{-2} (——) with $0.8502 \sin\psi$ (------).

(*a*) *The reconstruction of simple monotonic potentials*

For these potentials the critical voltage most frequently measured corresponds to a degeneracy of Bloch waves (2) and (3) so that A_{22} vanishes. In this case, the function $f_2(\psi)$ is often well approximated by the first term $A_{21}\sin\psi$ of the Fourier series (6.6), as shown in figure 18. With this simple approximation, the potential given by equations (6.4) and (6.5) is determined by only the two quantities $\gamma_c^{(n)}$ and A_{n1} and decreases from 0 to $\frac{1}{2}a$, provided that $\gamma_c^{(n)}$ and A_{n1} are both positive. However, to determine A_{n1} we need more information than critical voltages alone can provide. The critical angle θ_c introduced by Berry (1971) immediately suggests itself (Berry *et al.* 1973; Buxton & Berry 1973) since it is directly related to the depth of the potential, i.e.

$$\theta_c = \frac{K_c}{k_0} = \frac{1}{k_0}\sqrt{(-\bar{U}(x))_{\max}}. \tag{6.9}$$

For the potentials considered here this is just $(1/k_0)\sqrt{(-\bar{U}(\frac{1}{2}a))}$, and we then find that A_{n1} is uniquely determined from

$$\frac{a^2\gamma_c^{(n)}\bar{U}_0(\frac{1}{2}a)}{n^2} = -2\pi^2 I_0^2(\tfrac{1}{2}A_{n1})\sinh A_{n1}, \tag{6.10}$$

where I_0 is the modified Bessel function of order zero.

This reconstruction scheme was tested by using the values of $\gamma_c^{(n)}$ obtained from the 'many-beam' computations and the value of $\bar{U}_0(\frac{1}{2}a)$ obtained by summing the Fourier series (2.3). Twelve potentials reconstructed in this way are shown in figure 19 *a–f* and figure 20 *a–f*. The solid lines are the initial potentials obtained from (2.3), while the dashed line is the potential reconstructed from $\gamma_c^{(2)}$ and $\bar{U}_0(\frac{1}{2}a)$. Where these are indistinguishable the latter is omitted, and, for Au (200) and Pb (200) at 93 K, a potential reconstructed from $\bar{U}_0(\frac{1}{2}a)$ and $E_c^{(4)}$ is also included as a ·–·–·–·– line. In terms of the Fourier coefficients $U_{2\pi/a}$ these reconstructions are accurate to within a few percent. The examples shown indicate that this reconstruction is in general less accurate at low temperatures.

To understand this, and why the method does not work well for Al (111) or Mo (110) at either temperature, we must consider the terms $A_{nm}\sin(m\psi)$ which were neglected. Defining

$$\left.\begin{aligned}\gamma \equiv \frac{m^2\gamma_c^{(n)}}{n^2} &= \left[\frac{m\pi}{2\int_0^{\frac{1}{2}a} \mathrm{d}x'\sqrt{[s_0-\bar{U}_0(x')]}}\right]^2,\\ s &\equiv \gamma s_0,\end{aligned}\right\} \tag{6.11}$$

and

it follows that

$$|A_{nm}(s_0)| = (4/\pi)\,|R(s,\gamma)| \tag{6.12}$$

so that the term $A_{nm}\sin m\psi$ in (6.6) can be neglected only if $|R(s,\gamma)|$ is small. If m/n is greater than unity, $|R(s,\gamma)|$ will in general be small, and there will be two eigenvalues s_m and s_{m+1} near s, which are separated by a small band gap given approximately by

$$\Delta s_m \equiv s_{m+1}-s_m = 2|R(s,\gamma)|\Big/\frac{\partial\Phi(s,\gamma)}{\partial s}. \tag{6.13}$$

For large s, i.e. large m, this gap and $|R(s,\gamma)|$ will indeed be very small (recall equation (6.8)), but even for $m = 3$, states (3) and (4) are very close, being solutions of (2.26) in the 'above barrier' region where $|T| \approx 1$. Moreover, at 293 K, s_0 is larger than the corresponding s_0 at a low temperature so that the gap Δs_3, lying nearer to $s_0 = 0$, is larger at the lower temperature and the reconstruction is less accurate. This is confirmed by detailed calculations relating Δs_m to $f_n(\psi)$ via equations (6.3), (6.12) and (6.13). If $f_2(\psi)$ is approximated by $A_{21}\sin\psi$ we find that

$$|A_{23}| \approx \frac{a^2}{3\pi^2}\Delta s_3\,\frac{I_0(A_{21})}{I_0^2(A_{21}/2)}, \tag{6.14}$$

so that $|A_{23}|$ is easily estimated as shown in table 5. For each element, $|A_{23}|$ is larger at 93 K than at 293 K, and the values for Al (111) and Mo (110) are abnormally large, explaining the inaccuracy of our reconstruction scheme in these cases. We therefore extended the scheme to include the term $A_{23}\sin 3\psi$ in the approximation for $f_2(\psi)$ and used Δs_3, as well as $\bar{U}_0(\frac{1}{2}a)$, to determine the coefficients A_{21} and A_{23}. The reconstructions of the Al (111) and Mo (110) potentials were greatly improved as shown in figure 21 *a–d*. Since equation (6.12) only gives us the modulus $|A_{23}|$, we need a separate argument to show that A_{23} is positive: for small s_0, inversion of (6.6) shows that $A_{23} > 0$, and the fact that there is no degeneracy of Bloch waves (3) and (4) for these potentials means that it is always positive.

We can also see why we obtained the reasonable reconstructions from $E_c^{(4)}$ shown in figure 19 and figure 20 by neglecting A_{42} and A_{43} when only A_{44} was known to be zero! Fortuitously, $\gamma_c^{(4)} \approx 4\gamma_c^{(2)}$ for these potentials of Au and Pb, so that at the s_0 corresponding to $\gamma_c^{(4)}$, A_{42} is almost

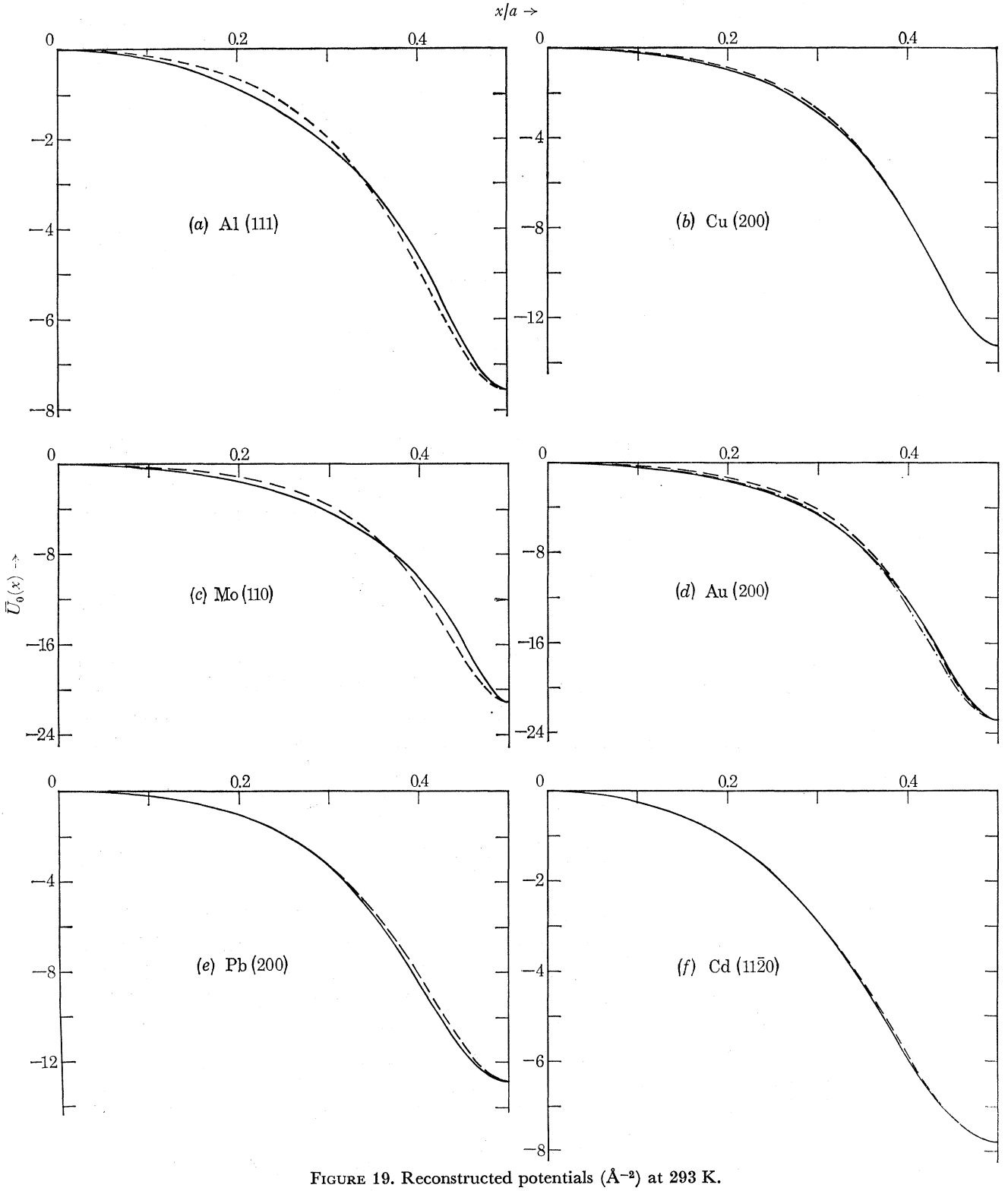

FIGURE 19. Reconstructed potentials (Å^{-2}) at 293 K.

PHILOSOPHICAL TRANSACTIONS OF THE ROYAL SOCIETY A MATHEMATICAL, PHYSICAL & ENGINEERING SCIENCES

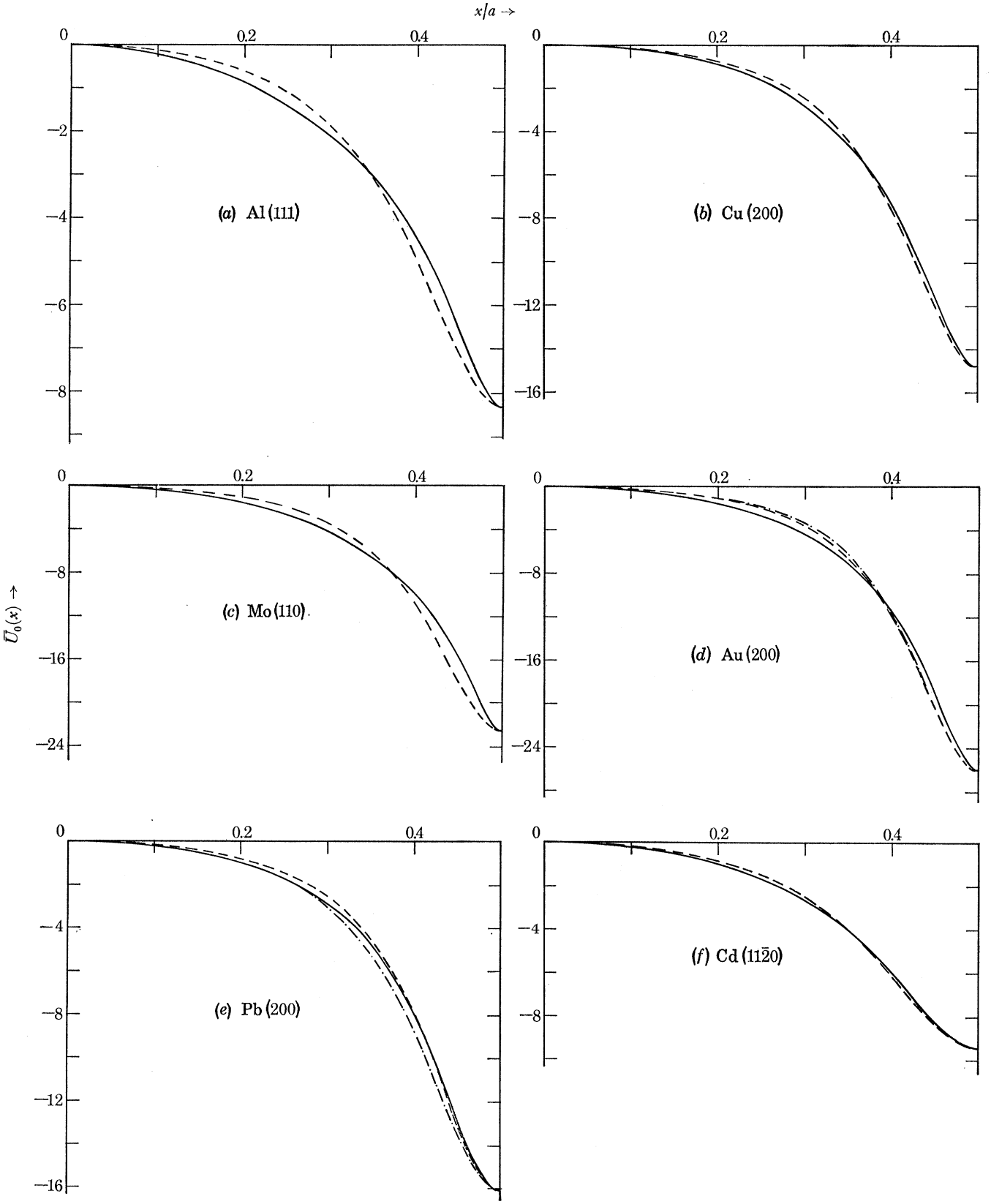

FIGURE 20. Reconstructed potentials (Å^{-2}) at 93 K, (*a*)–(*e*), and at 86 K (*f*).

PHILOSOPHICAL TRANSACTIONS OF THE ROYAL SOCIETY A MATHEMATICAL, PHYSICAL & ENGINEERING SCIENCES

TABLE 5. AT THE APPROPRIATE ENERGY $E = m_0c^2(\frac{9}{4}-1)+\frac{9}{4}E_c^{(2)}$ (cf. (6.11)), THE SEPARATION ΔS_3 OF BRANCHES 3 AND 4 OF THE DISPERSION SURFACE AT AN ODD BRAGG ORIENTATION WAS OBTAINED FROM A MATRIX SOLUTION OF THE 'MANY-BEAM' EQUATIONS. THE APPROXIMATE VALUES OF $|A_{23}|$ OBTAINED AS DISCUSSED IN THE TEXT ARE ALSO SHOWN

element (reflexion)	293 K			93 K		
	E	ΔS_3	$\lvert A_{23}\rvert$	E	ΔS_3	$\lvert A_{23}\rvert$
Al (111)	1705	0.659607	0.132	1876	1.015332	0.205
Cu (200)	2185	0.256354	0.031	2443	0.836818	0.105
Mo (110)	804	0.920186	0.174	847	1.149558	0.221
Au (200)	866	0.522053	0.083	1008	1.198053	0.197
Pb (200)	684	0.126028	0.028	997	0.380179	0.090

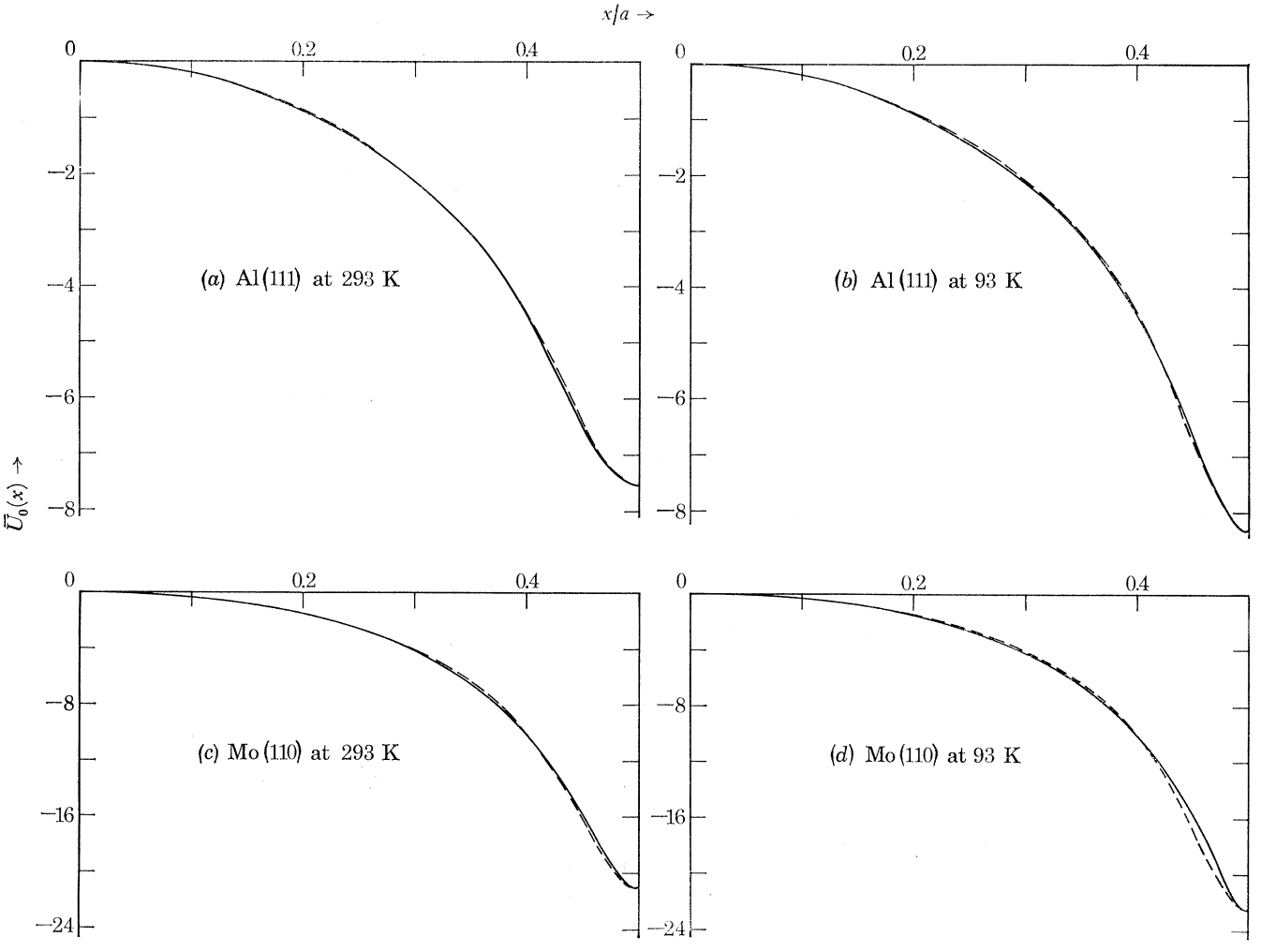

FIGURE 21. Reconstructions of the Al (111) and Mo (110) potentials (Å^{-2}) by using $f_2(\psi) \simeq A_{21}\sin\psi + A_{23}\sin 3\psi$.

zero, and the simple reconstruction works. This conclusion is strengthened by the fact that equation (6.10) for A_{n1} contains only $\gamma_c^{(n)}/n^2$.

Finally, we note that although $\gamma_c^{(2)}$ can be measured very accurately, the accuracy with which θ_c can be measured, either from bend contours or from the diffraction pattern has yet to be determined (Berry 1971; Richards & Steeds 1971; Berry *et al.* 1973). On the other hand, Δs_m is inversely proportional to the extinction distance $\xi_{m,m+1}$ (see, for example, Hirsch *et al.* 1965; Howie 1969) and should be easy to measure from the thickness fringes of a bent wedge shaped specimen (Richards 1973; Steeds *et al.* 1973).

(*b*) *Reconstruction from a 'pair' of critical voltages*

We saw in § 5 (i) that for some of these simple potentials two of the higher Bloch waves could degenerate at two different voltages. Obviously, the simplest reconstruction obtained by approximating $f_n(\psi)$ by $A_{n1}\sin\psi$ will not be suitable for these critical voltages, unless as just mentioned

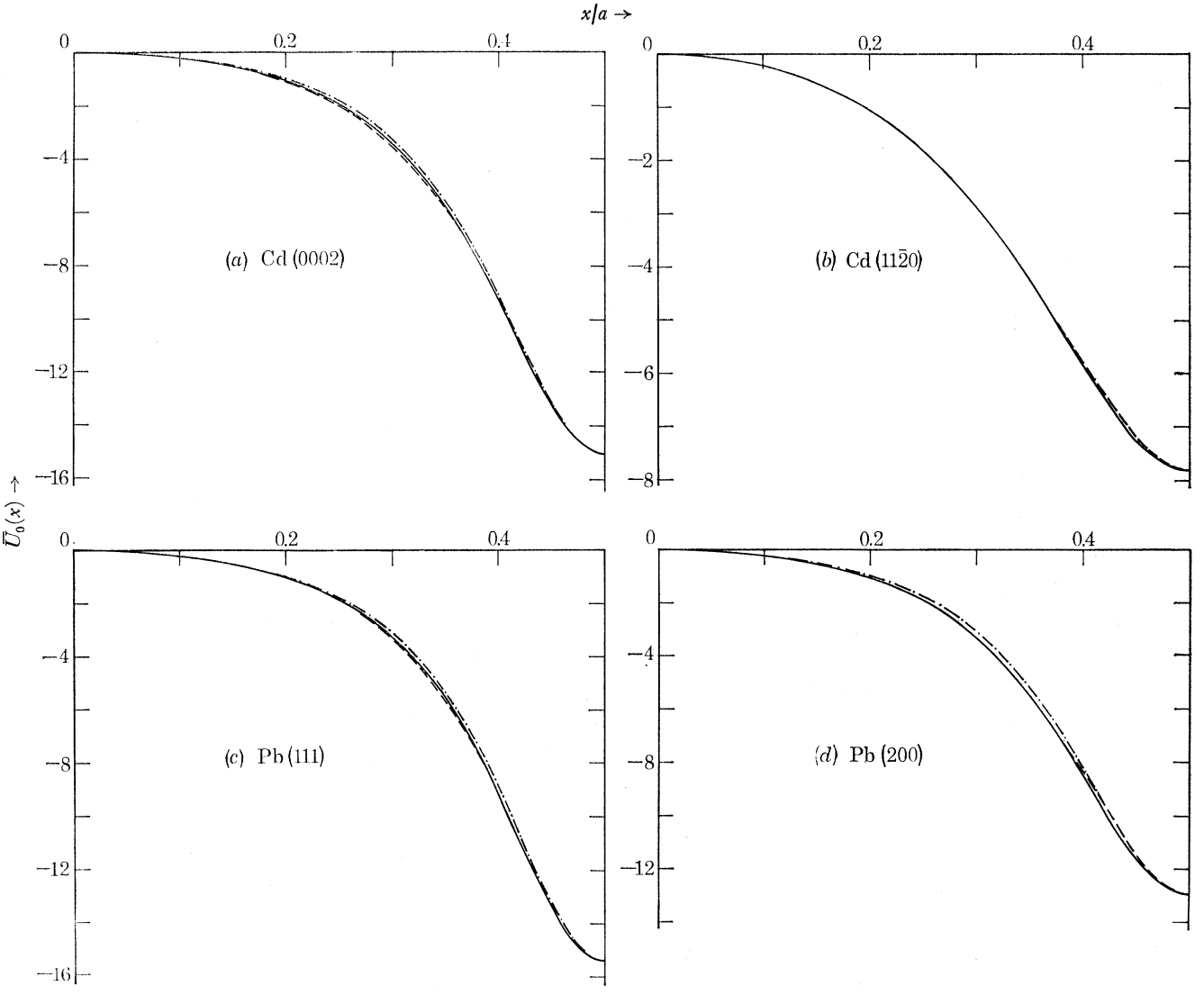

FIGURE 22. Reconstruction of four potentials (Å^{-2}) of cadmium and lead at 293 K from 'pairs' of values of $E_c^{(3)}$ (each reconstruction simultaneously generates two potentials shown as ------ and —·—·—).

A_{n2} fortuitously vanishes. The high values of these critical voltages (see table 2) indicate that the degeneracy of Bloch waves (3) and (4) is likely to be of most importance, so we approximate

$$f_3(\psi) = A_{31}\sin\psi + A_{32}\sin 2\psi, \tag{6.15}$$

with *different* values of the coefficients A_{3m} at each critical voltage.

Fitting each of the potentials generated from the two functions $f_3(\psi)$ to have the depth $\bar{U}_0(\frac{1}{2}a)$ at $\psi = \pi$ gives two equations similar to (6.10). To obtain two more equations which will completely determine the four coefficients we use the fact that it is the *same* potential $\bar{U}_0(x)$ which gives rise to these degeneracies, and insist that the reconstructed potentials have the same curvatures at $x = 0$ and at $x = \frac{1}{2}a$. This gives a pair of linear equations which can be solved for the A_{32} coefficients, a fact which greatly facilitates the numerical solution of our four (nonlinear) equations. The results are shown in figure 22 for four potentials at 293 K. The values of $E_c^{(3)}$ used were taken from the 'many-beam' results given in table 2, except for Cd $(11\bar{2}0)$ for which $E_c^{(3)} = 2054$ kV and 2908 kV at 293 K. Since two terms were retained in the approximation (6.15), these reconstructions are, on the whole, more accurate than those shown in figure 19 and figure 20, the Fourier coefficients $U_{2\pi/a}$ being reproduced to within about 1 %.

(*c*) *The* (111) *potential of silicon*

Before dealing with this more complicated case, let us discuss a few qualitative features of the function $f_n(\psi)$. In particular it is easily shown that

$$f_n(\psi) = 0 \Leftrightarrow \frac{\mathrm{d}\bar{U}_0(x)}{\mathrm{d}x} \equiv \bar{U}_0'(x) = 0, \tag{6.16}$$

and that at such points of zero force we have

$$\bar{U}_0''(x) = \frac{-n^2}{4\gamma_c^{(n)}a} f_n'(\psi)\left[\int_0^{\pi}\mathrm{d}\psi'\exp\left\{-\frac{1}{2}\int_0^{x'}\mathrm{d}x''f_n(\psi'')\right\}\right]^4 \exp\left\{\int_0^{\psi}\mathrm{d}\psi' f_n(\psi')\right\}. \tag{6.17}$$

The shape of the potential is therefore largely determined by the zeros of $f_n(\psi)$ and its slope at these points. In the case of the potentials previously dealt with which were monotonic for x in $[0, \frac{1}{2}a]$, the higher terms in the Fourier series (6.6) all had small coefficients to avoid introducing spurious stationary points into $\bar{U}_0(x)$. In the case of the (111) potential of silicon however it is essential that some of these coefficients are large so that a minimum near $x = 3a/8$ (see figure 12) can be generated. We therefore retained two terms in (6.6) and approximated $f_3(\psi)$ as in (6.15) for this reconstruction, using the critical voltages $E_c^{(3)}$ given in table 3.

However, there is a difficulty here in that we cannot use equations (6.12) and (6.13) to obtain A_{32}, since the latter is only valid if the band gap is small, and if s_{m+1} and s_m are positive. For silicon (111), it turns out that at an even Bragg position and at the appropriate beam voltage fixed by (6.11), s_2 is negative, s_3 positive and the gap Δs_2 very large so that the previous scheme breaks down. We therefore carried out a cruder reconstruction, assuming that the minimum in the potential occurs at $x = 3a/8$ (this is the position of the atomic planes as shown in figure 12) and obtained the encouraging results shown in figure 23. This procedure can then be improved as usual by including information from the higher band gaps Δs_4, etc. Indeed, we included terms up to $A_{35}\sin 5\psi$ in the approximation for $f_3(\psi)$ and determined the four unknown coefficients from the position and depth of the minimum in the potential and Δs_4 and Δs_5, to obtain the accurate reconstruction shown in figure 24.

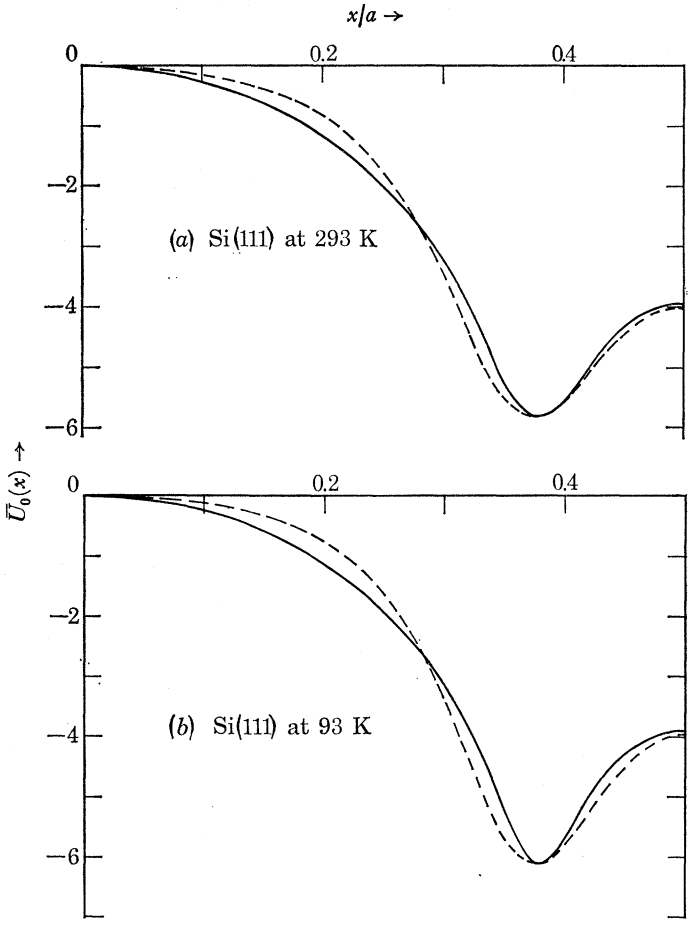

FIGURE 23. Reconstructions of the Si (111) potential (Å^{-2}) by using approximation (6.15) for $f_3(\psi)$, (*a*) at 293 K, (*b*) at 93 K.

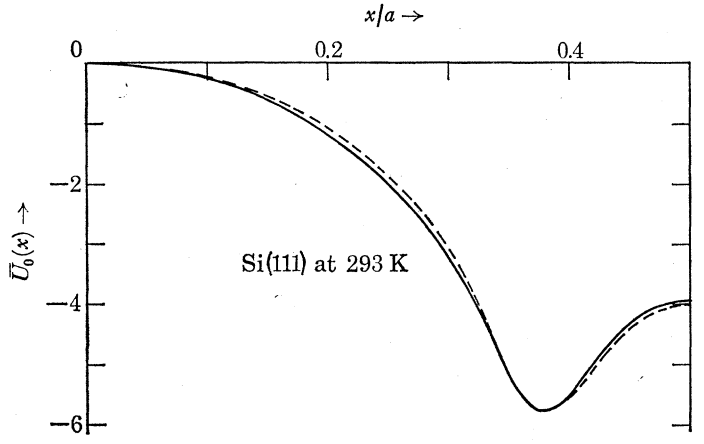

FIGURE 24. More accurate reconstruction of the Si (111) potential (Å^{-2}) at 293 K as described in the text.

PHILOSOPHICAL TRANSACTIONS OF THE ROYAL SOCIETY A MATHEMATICAL, PHYSICAL & ENGINEERING SCIENCES

(*d*) *The three dimensional potential* $U_0(\boldsymbol{r})$

Having shown how we can directly reconstruct the systematic potentials $\bar{U}_0(x)$ in real space in terms of a few simple parameters, let us now consider the full three dimensional potential $U_0(\boldsymbol{r})$, which can be expressed as a sum over the systematic potentials:

$$U_0(\boldsymbol{r}) - U_0^0 = \sum_{\hat{\boldsymbol{x}}} \{\bar{U}_0(\boldsymbol{r}\cdot\hat{\boldsymbol{x}}) - \langle \bar{U}_0(\boldsymbol{r}\cdot\hat{\boldsymbol{x}})\rangle\}. \tag{6.18}$$

$\sum_{\hat{\boldsymbol{x}}}$ represents the sum over all the systematic directions denoted by the unit vectors $\hat{\boldsymbol{x}}$, and the mean potentials U_0^0 and $\langle \bar{U}_0(\boldsymbol{r}\cdot\hat{\boldsymbol{x}})\rangle$ are included because a different choice of the zero of energy was made for each systematic potential (see § 2 (*a*)). The infinite sum (6.18) can be truncated by neglecting all systematic potentials for which the lattice plane spacing a is less than some detail size $|\Delta\boldsymbol{r}|$, and then reduced by using the crystal symmetry of $U_0(\boldsymbol{r})$. In general though there will be many weak potentials in the sum (6.18) which cannot be reconstructed in the way we have just described because the critical voltages are inaccessibly high. However, these potentials will only involve high order Fourier coefficients and can therefore be obtained quite accurately from the free atom calculations of Doyle & Turner (1968) (say) if we include a Debye–Waller factor to allow for the thermal vibrations of the atoms. In this way, the reconstruction of a few of the strongest systematic potentials should allow us to infer $U_0(\boldsymbol{r})$, without recourse to any assumptions about overlapping spherically symmetric potentials for these, the largest contributions.

We emphasize here that $U_0(\boldsymbol{r})$ is an optical potential and therefore includes a very small contribution due to virtual inelastic processes (Yoshioka 1957; Dederichs 1972) as well as a 'smearing out' due to the thermal motions of the atoms in the crystal. However, to a very good approximation, $\nabla^2 U_0(\boldsymbol{r})$ is proportional to the charge density in the crystal averaged over these thermal vibrations. Hence, we obtain information about the charge density of the idealized static crystal in the important interstitial region where it differs little from the thermally averaged charge density if this is spatially slowly varying.

7. Conclusions

These fall naturally into three groups, the first drawn from the exact treatment of §§ 2 and 3, the second concerning the semiclassical approximations used in §§ 4 and 5, and the third relating to the reconstruction scheme of § 6.

(*a*) *The exact formulation*

The most important fact is that the degeneracies are *accidental*. Only the novel feature of the scaling of the potential with the relativistic factor γ makes the critical voltage effect occur, and even this only for symmetric potentials (see the appendix). As is well known, the degeneracies occur at the Bragg positions where for a symmetric potential non-degenerate Bloch waves can be assigned a definite parity. We showed how the ordering of the parities of the Bloch waves with increasing eigenenergy s_j depended on the location of the zeros of the reflexion coefficient $R(s)$, and that at a degeneracy these parities could be interchanged. Indeed, this exchange of parities is essential, because no degeneracies occur for the bound ($s_j < 0$) states, and for simple monotonic potentials they alternate in parity as we look at states of progressively higher s_j. The parities of the states with positive s_j however usually differ from this strictly alternating series, and without a

degeneracy, and the interchange of parities, these states would not be able to pass smoothly into the bound region as the potential is deepened by an increase in the relativistic factor γ. We also saw that, where $R(s)$ had a higher order zero, a higher order degeneracy could occur without a change in the symmetries of the Bloch states.

In § 3, the energy bands were found to be hyperbolic near a degeneracy, and to become a line pair and *cross* at the critical γ_c. Also, near γ_c we saw that the Bloch waves themselves depend strongly on the orientation, changing from a travelling wave form far from the Bragg position to a standing wave form at the Bragg position. It was shown that this gave rise to a characteristic rapid change in the Fourier coefficient of the Bloch waves, and to lead to a few complications when absorption effects are included by perturbation theory. We then showed *analytically* how the degeneracy and the rapid changes in the Fourier coefficients account for the well-known 'critical voltage effects' visible in the diffracted waves and the Kikuchi pattern.

(*b*) *The semiclassical approximations*

In § 4 we used W.K.B. approximations to show that the Bragg orientation K_0^B could be chosen so that the excitations of the degenerate Bloch waves were comparable and *large*, and in § 4 (*a*) that they would often also have comparable and *small* absorption coefficients. In this way, it became clear how the contributions from these Bloch waves could dominate some of the diffracted beam intensities and the Kikuchi pattern and so lead to observable effects at the degeneracy. We found, however, that a W.K.B. formula for the transmission coefficient $T(s)$ could not describe the degeneracies and used instead a formula for $R(s)$, due to *Landauer*. This led to simple equations (4.13) and (4.14) for the critical s_c and γ_c, which we used in §§ 4 (*c*) and (*d*) to understand how γ_c varied with temperature and which Bloch waves could degenerate for a given form of potential.

In § 5, it was shown by comparison with exact 'many-beam' calculations that numerical solutions of these same equations gave accurate estimates of the critical voltages. Moreover, they even predicted accurately the occurrence of higher order degeneracies in lead, cadmium and gold. At the end of this section, we emphasized that the higher order degeneracies, which only occurred by chance as γ alone was varied could be made to occur for many values of γ by varying γ and the temperature simultaneously.

(*c*) *The reconstruction scheme*

Finally (§ 6), we used the simplicity and accuracy of the semiclassical formulae to derive an inversion technique. Initially, this depended only on a measurement of critical voltage for a degeneracy of Bloch waves (2) and (3), and on a measurement of a critical angle. However, it was systematically improved by the addition of information derived from extinction lengths at Bragg positions, and then extended to include other critical voltages. This scheme gives the crystal potential directly in real space without using additional calculated information or making any assumptions about overlapping spherical atoms. However, it is less accurate than the conventional determination of atomic scattering factors (see, for example, Thomas *et al.* 1973).

Nevertheless, as the example with the more complicated potential of Si (111) systematics showed, its strength lies in its simplicity and the direct way it is related to the shape (i.e. number of minima) of the potential. This could mean that a fairly rough reconstruction would be useful when attempting to analyse an unknown structure.

PHILOSOPHICAL TRANSACTIONS OF THE ROYAL SOCIETY A MATHEMATICAL, PHYSICAL & ENGINEERING SCIENCES

It is a pleasure to thank Dr J. W. Steeds for many helpful discussions and also Dr I. P. Jones and Dr E. A. Hewat for their useful suggestions. One of us (B. F. B.) wishes to thank the Science Research Council for a Research Studentship and a Research Fellowship.

Appendix

Critical voltages for an asymmetric potential

The question of interest here is whether a variation of the relativistic factor γ offers enough scope to ensure that a degeneracy of a pair of Bloch waves will occur. We shall show that for a general asymmetric potential it does not, i.e. even as γ is varied degeneracies will occur only by chance. For such a potential the reflexion coefficients R_{L} and R_{R} of waves τ_{L} and τ_{R} incident from the left and right respectively (as in figure 1) are not the same, but using the properties of the Wronskian (see, for example, Messiah 1962, vol. 1) it is easy to show that we can write

$$\left.\begin{aligned} T &= |T|\,\mathrm{e}^{\mathrm{i}\delta}, \\ R_{\mathrm{L}} &= |R|\,\mathrm{e}^{\mathrm{i}(\nu_{\mathrm{L}}+\delta)}, \\ R_{\mathrm{R}} &= |R|\,\mathrm{e}^{\mathrm{i}(\nu_{\mathrm{R}}+\delta)}, \end{aligned}\right\} \tag{A 1}$$

where

$$\nu_{\mathrm{L}}+\nu_{\mathrm{R}} = (2p+1)\,\pi, \quad p = 0, \pm 1, \pm 2, \ldots \tag{A 2}$$

and hence that the band structure equations (2.12) and (2.15) are the same, when expressed in terms of these scattered waves, as for a symmetric potential.

Thus for a degeneracy we must have $|R| = 0$, i.e.

$$\mathrm{Re}\,R = \mathrm{Im}\,R = 0 \tag{A 3}$$

and also

$$\beta\alpha+\delta = n\pi. \tag{A 4}$$

With only two variables s and γ, we cannot satisfy all three of the conditions above, except by chance. The best we can hope for is to minimize $|R|$, or to reduce the separation of two of the energy bands to a minimum. Perhaps, by varying the temperature of the specimen, this minimum could be reduced to zero and a critical voltage for an asymmetric potential obtained in a similar way to the higher order degeneracies of symmetric potentials.

For a symmetric potential the essential point is that $R_{\mathrm{L}} = R_{\mathrm{R}}$, so that

$$\nu_{\mathrm{L}} = \nu_{\mathrm{R}} = (2p+1)\,\tfrac{1}{2}\pi, \tag{A 5}$$

and the real and imaginary parts of R are no longer independent functions, since

$$\mathrm{Re}\,R = \mathrm{Im}\,R\tan\left(a\sqrt{[s-\gamma\bar{U}_0(\tfrac{1}{2}a)]}\right), \tag{A 6}$$

and we only have two conditions in (A 3) and (A 4) which must be satisfied at a degeneracy.

References

Abramowitz, M. & Stegun, I. A. S. 1964 *Handbook of mathematical functions*. Washington: U.S. National Bureau of Standards.

Aldred, P. J. E. 1971 Ph.D. Thesis, University of Bristol.

Andrew, J. N. & Sheinin, S. S. 1974 *Proc. 8th International Congress on Electron Microscopy*, vol. 1, pp. 338–339. Canberra: Australian Academy of Science.

Berry, M. V. 1971 *J. Phys.* C **4**, 697–722.

Berry, M. V. & Mount, K. E. 1972 *Reps. Prog. Phys.* **35**, 315–397.

Berry, M. V., Buxton, B. F. & Ozorio de Almeida, A. M. 1973 *Radiation Effects* **20**, 1–24.
Buxton, B. F. & Berry, M. V. 1973 *Proc. 3rd International Conference on High Voltage Electron Microscopy*, pp. 60–63. London & New York: Academic Press.
Dederichs, P. H. 1972 *Solid State Phys.* **27**, 135–236.
Doyle, P. A. & Berry, M. V. 1973 *Z. Naturforsch.* **28***a*, 571–576.
Doyle, P. A. & Turner, P. S. 1968 *Acta Cryst.* A **24**, 390–397.
Erdélyi, A. 1956 *Asymptotic expansions*. New York: Dover.
Fujiwara, K. 1961 *J. Phys. Soc. Japan* **16**, 2226–2238.
Fujiwara, K. 1962 *J. Phys. Soc. Japan* **17**, Suppl. B-II, 118–123.
Hirsch, P. B., Howie, A., Nicholson, R. B., Pashley, D. W. & Whelan, M. J. 1965 *Electron microscopy of thin crystals*. London: Butterworths.
Høier, R. 1972 *Phys. Stat. Sol.* (*a*) **11**, 597–610.
Høier, R. 1973 *Acta. Cryst.* A **29**, 663–672.
Howie, A. 1969 In *Modern diffraction and imaging techniques in material science* (eds. S. Amelinckx, R. Gevers, G. Remaut & J. Van Landuyt), pp. 295–339. Amsterdam: North-Holland.
International Tables for X-ray Crystallography 1965 Birmingham: Kynoch Press.
Jones, I. P. & Tapetado, E. G. 1973 *Proc. 3rd International Conference on High Voltage Electron Microscopy*, pp. 48–51. London, New York: Academic Press.
Jones, H. 1960 *The theory of Brillouin zones and electronic states in crystals*. Amsterdam: North-Holland.
Kohn, W. 1959 *Phys. Rev.* **115**, 809–821.
Kramers, H. A. 1935 *Physica* **2**, 483–490.
Lally, J. S., Humphreys, C. J., Metherell, A. J. F. & Fisher, R. M. 1972 *Phil. Mag.* **25**, 321–343.
Messiah, A. 1962 *Quantum mechanics*, vol. 1. Amsterdam: North-Holland.
Metherell, A. J. F. & Fisher, R. M. 1969 *Phys. Stat. Sol.* **32**, 551–562.
Nagata, F. & Fukuhara, A. 1967 *Japan, J. appl. Phys.* **6**, 1233–1235.
Pokrovskii, V. L., Ulinich, F. R. & Savvinykh, S. K. 1958 *Sov. Phys. J.E.T.P.* **34**, 1119–1120.
Richards, C. J. 1973 Ph.D. Thesis, University of Bristol.
Richards, C. J. & Steeds, J. W. 1971 *Proc. 25th Anniv. Meeting E.M.A.G.*, pp. 128–131. London, Bristol: Institute of Physics.
Rocher, A. & Jouffrey, B. 1972 *Proc. 5th European Congress on Electron Microscopy*, pp. 528–529. London, Bristol: Institute of Physics.
Scharff, M. 1969 *Elementary quantum mechanics*. London: Wiley-Interscience.
Sheinin, S. S. & Cann, C. 1973 *Phys. Stat. Sol.* (*b*) **57**, 315–320.
Shirley, C. G., Lally, J. S., Thomas, L. E. & Fisher, R. M. 1975 *Acta. Cryst.* A **31**, 174–177.
Sprague, J. A. & Wilkins, M. 1970 *Septième Congrès International de Microscopie Électronique*, pp. 95–96. Paris: Société Française de Microscopie Électronique.
Steeds, J. W. & Enfield, A. C. 1971 *Proc. 25th Anniv. Meeting E.M.A.G.*, pp. 126–127. London, Bristol: Institute of Physics.
Steeds, J. W., Tatlock, G. J. & Hampson, J. 1973 *Nature, Lond.* **241**, 435–438.
Thomas, L. E. 1972 *Phil. Mag.* **26**, 1447–1465.
Thomas, L. E., Shirley, C. G., Lally, J. S. & Fisher, R. M. 1973 *Proc. 3rd International Conference on High Voltage Electron Microscopy*, pp. 38–47. London, New York: Academic Press.
Watanabe, D., Uyeda, R. & Fukuhara, A. 1968 *Acta. Cryst.* A **24**, 580–581.
Watanabe, D., Uyeda, R. & Kogiso, M. 1968 *Acta. Cryst.* A **24**, 249–250.
Yoshioka, H. 1957 *J. Phys. Soc. Japan* **12**, 618–628.

PHILOSOPHICAL TRANSACTIONS OF THE ROYAL SOCIETY A MATHEMATICAL, PHYSICAL & ENGINEERING SCIENCES